Epitaxial growth in dislocation-free strained asymmetric alloy films

Rashmi C. Desai,* HoKwon Kim,† Apratim Chatterji,‡ Darryl Ngai,§ Si Chen,‖ and Nan Yang¶
Department of Physics, University of Toronto, Toronto, Ontario, Canada M5S 1A7
(Received 26 February 2010; revised manuscript received 3 May 2010; published 1 June 2010)

Epitaxial growth in strained *asymmetric*, dislocation-free, coherent, alloy films is explored. Linear-stability analysis is used to theoretically analyze the coupled instability arising jointly from the substrate-film lattice mismatch (morphological instability) and the spinodal decomposition mechanism. Both the static and growing films are considered. Role of various parameters in determining stability regions for a coherent growing alloy film is investigated. In addition to the usual parameters: lattice mismatch ϵ, solute-expansion coefficient η, growth velocity V, and growth temperature T, we consider the alloy asymmetry arising from its mean composition. The dependence of elastic moduli on composition fluctuations and the coupling between top surface and underlying bulk of the film also play important roles. The theory is applied to group III-V films such as GaAsN, InGaN, and InGaP and to group IV Si-Ge films at temperatures below the bare critical temperature T_c for strain-free spinodal decomposition. The dependences of various material parameters on mean concentration and temperature lead to significant qualitative changes.

DOI: 10.1103/PhysRevB.81.235301 PACS number(s): 68.35.Fx, 68.55.J−, 81.15.Aa, 81.15.Hi

I. INTRODUCTION

A dislocation-free coherent film can be grown on top of a substrate using a variety of experimental techniques. The growth of such a film is based on the atomic pattern of the substrate underneath, as if it is an extension of the substrate structure; such a growth is termed an epitaxial growth. In heteroepitaxy, the material of the film is different than that of the substrate. The ability to grow such solid thin films has been of central importance in the development of modern electronic and optical devices.

In order to produce good quality thin solid layers during the epitaxial growth, a near match of the lattice spacings of the film and the substrate is desirable since it minimizes and possibly eliminates local strains in the film. In alloy films, the mean composition can be tuned to obtain a desired band gap and also to match the substrate-film lattice spacing for some systems. However, for the film to be useful, its composition needs to remain homogeneous. The stability of a film, grown using a typical technique such as molecular-beam epitaxy (MBE), depends on many variables. The process of epitaxial growth is a nonequilibrium phenomenon in which elastic energy, surface energy, and interfacial energy are central; surface diffusion, deposition rate of film materials and alloy segregation also play active roles.

During the growth, dislocations or other defects may get nucleated in the film to relieve accumulated strain. The generation of dislocations can be avoided through inhomogeneities in the film, which can arise due to two potential instabilities: morphological instability and alloy segregation instability, the former resulting from substrate-film lattice mismatch and the latter from spinodal decomposition mechanism.

The dislocation-free morphological instability is a process during which the growth mode of the film changes from a two dimensional "layer-by-layer" to three dimensional, still keeping the film coherent with the substrate. The morphological instability occurs in many heteroepitaxial systems has been well-understood theoretically[1–4] and has also been reviewed[5–7] for single-component films. The gist of this instability can be summarized as follows. The planar surface of a nonhydrostatically stressed solid, such as the epitaxially growing alloy film, is unstable to the formation of surface corrugations: if a small corrugation occurs, local strain energy concentration is created at its valley; this leads to diffusion of matter along the film surface from the valley to a neighboring peak where the strain energy is lower, which, in turn, deepens the valley due to loss of mass, which then leads to a further increase in local strain energy, thus driving the instability. The deepening corrugations increase the surface area with an associated surface-energy cost inhibiting the growth of instability; the surface energy thus plays a stabilizing role.

The alloy-segregation instability is driven by the thermodynamics of spinodal decomposition[8] and is typically modeled by a Landau-Ginzburg-type free energy in which the order parameter is related to the binary-alloy concentration and in which the coefficient of the quadratic term is proportional to $(T-T_c)$. Here T_c is the bare critical temperature. For $T<T_c$, this term changes sign and leads to the spinodal decomposition instability which results in a segregation of a homogeneous mixture if its mean concentration is within the classical spinodal. In this paper, we consider epitaxial growth in strained, *asymmetric*, dislocation-free, coherent alloy films. Stability of alloy films has been theoretically considered previously[4,9–26] where, by and large, attention has been focused either on symmetric films or on films at temperatures larger than T_c or both. In this paper, we concentrate on asymmetric, binary or pseudobinary alloys with $T<T_c$.

Composition modulations and inhomogeneities have been seen experimentally in many alloy films: among them in $In_xGa_{1-x}As_yP_{1-y}/InP$ (Refs. 27–29) as early as 1982; in InGaP;[30–32] Al-Ge;[33] $Zn_xMg_{1-x}Se_yS_{1-y}$;[34] AlGaN and InAlGaN;[35] InGaN;[36–39] InGaAs;[40,41] and many multilayers including AlAs/InAs multilayers.[42]

The alloy film that has been most extensively studied experimentally is Si-Ge on a Si substrate.[43–55] For the Si-Ge alloy, T_c is around 260 K and almost all the experiments are done at $T>T_c$; at these temperatures, only the morphological

instability is relevant and has been very effectively used to create self-assembled nanostructures.[43] In contrast, two nitride alloys GaAsN and InGaN and the alloy InGaP have T_c larger than 1000 K. Each of these three pseudobinary alloy films has been experimentally studied and composition inhomogeneities have been seen. For nitride semiconductor alloys, there has been a burst of experimental activity due to their potential application to devices.[56,57] For all the semiconductor films, there is a growing realization that the inherent instability in the growth mechanism of the constituent materials can be used to enable the system to self-assemble and form nanostructures.[6,57]

The group III-V nitrides have interesting properties which are far removed from all other semiconductor compounds, e.g., N incorporation in GaAs (forming GaAsN) results in an important band-gap change which opens the possibility of designing new optoelectronic devices with novel properties; these include high-efficiency solar cells.[58,59] The large difference in the lattice constants of pure GaAs and GaN leads to an extensive miscibility gap between the two compounds and results in a large band gap. The width of the bandgap is tunable by having different compositions x in the $GaAs_{1-x}N_x$ pseudobinary alloy. However, the significant elastic energies resulting from the large difference in the lattice constants of GaAs and GaN constituents also make it extremely difficult to grow a coherent GaAsN film on a GaAs substrate. Even though, nitrogen solubility in GaAs can be significantly higher in epitaxial films compared to bulk,[59,60] it is difficult to incorporate more than 10% ($x>0.1$) of N in GaAs without the roughening of the surface accompanied by phase segregation of the two components.[61,62] Morphology and optical properties of GaAsN film on GaAs substrate have also been explored as part of a study of GaInAsN films.[63] InGaN and AlGaN are among pseudobinary nitride alloys that have also contributed to the development of a new generation of light emitters due to their efficient luminescence. By adjusting InN content in an InGaN/GaN film, most of the visible spectral region can be covered. The role of nanoscale strain inhomogeneity on the light emission from InGaN epitaxial films has been described by Pereira *et al.*[36] Growth of flat GaN films at low temperatures under Ga-rich conditions has met with moderate success indicating sensitive dependence of the film stability on temperature T. Overall the experiments show that stressed films can develop nonplanar morphology without dislocations or nucleation. The onset of instability is measured through a kinetic critical thickness ℓ_c, at which surface roughening first appears, and through the characteristic wavelength of instability λ.

In this paper, we extend the continuum nonequilibrium model of Huang and Desai[25] to asymmetric alloy films and apply it to some group III-V semiconductor films. The model is described in Sec. II with many of its details given in Appendices A and B. The model includes the coupling between top surface, underlying bulk of the growing film, and the substrate underneath; this coupling arises from elastic forces; composition dependence of the elastic constants that enter the elastic energy is also included. The alloy segregation instability is built in the model through a Landau-Ginzburg model free energy which fully incorporates the asymmetry of the binary or pseudobinary alloy films. The stabilizing surface energy is included through its simplest possible model, the drumhead model, with isotropic surface tension. There are many parameters in the model, but none is adjustable. The dependence of these parameters on temperature T and mean alloy concentration x [through $\phi_o(=2x-1)$] is discussed at the end of Sec. II. Linear stability analysis of the model is presented in Sec. III in which various limiting cases, including that of static films, are discussed before the consideration of the general case. The manner in which the general case can be numerically applied to a specific film is illustrated for SiGe/Si film at 200 K. In Sec. IV, the theory is applied to asymmetric nitride films GaAsN/GaAs and InGaN/GaN and to asymmetric InGaP/GaAs film. Finally, we conclude with a summary discussion in Sec. V. The theory described in this paper can improve our understanding of the inherent dynamical phenomenon in the growth of epitaxial alloy films, since it is a theory based on fundamental principles with predictive power about the optimum growth conditions. For binary alloy films, with critical temperature larger than 1000 K, at typical growth temperatures (500–900 K), the constituent materials tend to phase segregate and diffuse on the top surface leading to the coupled morphological and phase-segregation instability. The interplay of the relative strengths of the morphological instability and the phase-segregation instability, and the effect of surface diffusion and material deposition in enhancing/suppressing the resultant coupling of these two instabilities are the key ingredients in the theory.

II. MODEL

The model system consists of a semi-infinite substrate occupying $-\infty<z<0$ on which a strained asymmetric binary (or pseudobinary) alloy film is coherently grown. The growing film lies within $0<z<h(x,y,t)$ where $h(x,y,t)$ is its instantaneous height above the substrate. We assume that evaporation and recondensation are negligible during the epitaxial growth of the film under ultrahigh-vacuum conditions. We also assume that the film completely wets the substrate, that no interdiffusion occurs between film and substrate, and that the diffusion in the bulk film is negligible compared to that on the surface. Due to deposition, the average height of the film $\bar{h}=vt$ grows linearly with time and the growth velocity $v=\Lambda N_s/N_v$, where Λ is the deposition rate (the number of atoms falling per unit time) and $N_s/N_v \equiv \delta$ is akin to the thickness of a monolayer; here N_s is the surface-number density (per unit area) and N_v is the volume-number density (per unit volume) of the film. Later in the paper, we also refer to δ as the interaction distance.

A. Equations of motion

The evolution of the film height follows a conserved dynamics. The motion of the interface satisfies a continuity equation

$$N_v \frac{\partial r_n}{\partial t} = -\nabla \cdot \mathbf{J}_h + \tilde{\Lambda}, \tag{1}$$

where $\partial r_n/\partial t$ is the rate of change in the interface position along its normal and $\tilde{\Lambda}=\Lambda N_s/\sqrt{g}$. The Cartesian components

of the normal unit vector $\hat{\mathbf{n}}$, pointing away from the film, are given by $(-\partial h/\partial x, -\partial h/\partial y, 1)/\sqrt{g}$, where $g=(1+|\nabla_s h|^2)$ is the determinant of the surface metric with $|\nabla_s h|^2=(\partial h/\partial x)^2+(\partial h/\partial y)^2$. Then the equation for the z component of the interface motion is

$$\frac{\partial h}{\partial t}=\sqrt{g}\frac{\partial r_n}{\partial t}=-N_v^{-1}\sqrt{g}\nabla_s\cdot\mathbf{J}_h+v. \tag{2}$$

Here the surface flux of atoms $\mathbf{J}_h$ is proportional to the gradient of a diffusion potential, $\delta\mathcal{F}/\delta h$

$$\mathbf{J}_h=-\frac{D_s N_s}{k_b T N_v}\nabla_s\frac{\delta\mathcal{F}}{\delta h}, \tag{3}$$

where $\mathcal{F}$ is the total free-energy functional of the system. From the above two equations, one has

$$\frac{\partial h}{\partial t}=\Gamma_h\sqrt{g}\nabla_s^2\frac{\delta\mathcal{F}}{\delta h}+v, \tag{4}$$

where ∇_s^2 is the surface Laplacian and $\Gamma_h=D_s N_s/(k_B T N_v^2)$ is the kinetic coefficient[64] which depends on N_s, N_v, temperature T, and surface-diffusion coefficient D_s. In a reference frame moving with the average surface position $\bar{h}$, one obtains

$$\frac{\partial\delta h}{\partial t}=\Gamma_h\sqrt{g}\nabla_s^2\frac{\delta\mathcal{F}}{\delta h}. \tag{5}$$

The evolution of the height fluctuation $\delta h(x,y,t)\equiv(h(\vec{x},t)-\bar{h})$ is coupled to local concentration fluctuation of the alloy through the free-energy functional $\mathcal{F}$. We denote (x,y) by $(\vec{x})$. It is convenient to introduce the local order-parameter field $\phi(\vec{x},z,t)=2c(\vec{x},z,t)-1$, where $c(\vec{x},z,t)$ is the instantaneous local concentration of component A in a A_xB_{1-x} alloy film; ϕ and c are defined only for $0<z<h(\vec{x},t)$. The order-parameter fluctuation $\delta\phi(\vec{x},z,t)=\phi(\vec{x},z,t)-\bar{\phi}$ plays a crucial role in the film's growth; here $\bar{\phi}=2x-1$ and x is the average concentration. If x is a fraction other than 0.5, then component A forms an asymmetric solid solution of composition x with B. Due to the neglect of diffusion in the bulk of the film, the layers within the film are buried metastable layers which are frozen. It implies that the bulk order-parameter field ϕ_b at some time t is equal to the surface field ϕ_s of an earlier time: $\phi_b(\vec{x},z,t)=\phi_s(\vec{x},t-t_o)$ for $0<z<h$, where $t_o\sim(\bar{h}-z)/v$. This, in turn, implies that $\phi_b(\vec{x},z,t)\sim\phi_s(\vec{x},t=z/v)$. The evolution of $\delta\phi(\vec{x},z,t)$ also follows a conserved dynamics and is given by

$$\frac{\partial\delta\phi}{\partial t}=\Gamma_\phi\nabla^2\frac{\delta\mathcal{F}}{\delta\phi}-\Lambda\delta\phi\Delta(z-h), \tag{6}$$

where

$$\Delta(z-h)=\begin{cases}1 & \text{if } z=h,\\ 0 & \text{elsewhere}\end{cases} \tag{7}$$

and where $\Gamma_\phi=D_s/(k_B T N_v)\equiv\Gamma_h\delta^{-1}$. Here $\delta=\Gamma_h/\Gamma_\phi=N_s/N_v$ is the effective diffusion thickness of the surface layer and $v=\Lambda\delta$. One can also view δ as an effective monolayer thickness. The second term on the right, in Eq. (6), results from the tendency of the surface composition to approach its average value.[24,65] We neglect the deposition noise and thermal noise since this neglect does not alter the results of a linear-stability analysis.[24] In order to obtain the surface order-parameter field ϕ_s, we take into account the coupling between the surface and the underlying bulk of the growing film in the same way as was done by Huang and Desai.[25]

B. Free-energy functional

The free-energy functional $\mathcal{F}$ of the entire system from $z=-\infty$ to h is the sum of the surface free energy $\mathcal{F}_s$, the Landau-Ginzburg free energy $\mathcal{F}_{\mathrm{LG}}$, and the elastic free energy $\mathcal{F}_{\mathrm{el}}(\phi,\mathbf{u},h)$

$$\mathcal{F}=\mathcal{F}_s+\mathcal{F}_{\mathrm{LG}}+\mathcal{F}_{\mathrm{el}}, \tag{8}$$

$$\mathcal{F}_s=\gamma\int dxdy\sqrt{g}, \tag{9}$$

$$\mathcal{F}_{\mathrm{LG}}=\int dx\int dy\int_0^h dz\left[-\frac{r'}{2}(\phi-\phi_c)^2+\frac{u}{4}(\phi-\phi_c)^4+\frac{\kappa}{2}(\nabla\phi)^2\right], \tag{10}$$

$$\mathcal{F}_{\mathrm{el}}(\phi,\mathbf{u},h)=\frac{1}{2}\int dx\int dy\int_{-\infty}^h dz S_{ijkl}\sigma_{ij}\sigma_{kl}=\frac{1}{2}\int dx\int dy\int_{-\infty}^h dz\lambda_{ijkl}u_{ij}u_{kl}. \tag{11}$$

We now describe $\mathcal{F}_s$, $\mathcal{F}_{\mathrm{LG}}$, and $\mathcal{F}_{\mathrm{el}}$ in sequence. The surface energy term $\mathcal{F}_s$, Eq. (9), is represented by a simple model, the drumhead model without any pinning term in which γ is the surface tension at the top surface; it is assumed to be isotropic. The case where γ may have a linear composition dependence does not lead to any extra contribution to the results of linear-stability analysis.[25] In a nonlinear theory and in multilayer films, it is important to include the anisotropy of γ, a nonlinear dependence of the surface energy on the strain tensor and the wetting effect arising from a nonlinear dependence on layer thickness.[6,42,66–68] We ignore these nonlinear effects due to our limited goal of a linear-stability analysis.

The Landau-Ginzburg free energy $\mathcal{F}_{\mathrm{LG}}$, Eq. (10), is an expansion around the bare critical point (ϕ_c,T_c). As will be seen below, the elastic free-energy renormalizes the location of the critical point.[8] Since one can write $(\phi-\phi_c)=(\phi-\bar{\phi})+(\bar{\phi}-\phi_c)\equiv\delta\phi+\phi_o$ with $\phi_o=(\bar{\phi}-\phi_c)$, we have

$$\mathcal{F}_{\mathrm{LG}}=\int dx\int dy\int_0^h dz\left[-\frac{r'}{2}(\delta\phi+\phi_o)^2+\frac{u}{4}(\delta\phi+\phi_o)^4+\frac{\kappa}{2}(\nabla\delta\phi)^2\right], \tag{12}$$

where u and κ are positive constants. In a mean-field theory

for a binary mixture, in thermodynamic equilibrium, the free energy per mole is $f_{mix}=x\log x+(1-x)\log(1-x)+\chi_r x(1-x)$. The critical point occurs at $x_c=1/2$ or $\phi_c=0$ and $T_c=\chi_r/(2R)$, where R is the universal gas constant. For example,[61] $\chi_r=2.16\times10^5$ J mol^{-1} for $GaAs_{1-x}N_x$, which corresponds to $T_c\simeq13\,000$ K. By expanding f_{mix} around the critical point and comparing the coefficients of the second and fourth order terms with those in Eq. (12), we obtain $u=k_BN_vT_c/3$ and $r'=k_BN_v(T_c-T)$; r' is positive for $T<T_c$. The number density of molecules in the film N_v is $8/a_f^3$ for group IV alloys (such as Si-Ge alloys) and $4/a_f^3$ for group III-V alloys,[17] where a_f is the lattice constant of the film's material in bulk. The surface number density N_s is $2/a_f^2$. The coefficient for the square gradient term is $\kappa=k_BT_cN_v\delta^2/2$ where the interaction distance is denoted by $\delta\equiv N_s/N_v$; it is $a_f/4$ for group IV alloys and $a_f/2$ for group III-V alloys. Since $\phi_c=0$, $\bar{\phi}=\phi_o$ is the average order parameter. In absence of fluctuations the integrand is the Landau free energy per unit volume $f_L=-(r'/2)\phi_o^2+(u/4)\phi_o^4$. Its first derivative $f_L'=-r'\phi_o+u\phi_o^3$ is the thermodynamic force conjugate to the order parameter and the second derivative $f_L''=-r'+3u\phi_o^2$ is the inverse susceptibility. Mean-field isotherms plotted in the f_L'-ϕ_o plane for $T<T_c$ show van der Waals loops and the locus of the extrema of the isotherms, given by $f_L''=0$, is the classical spinodal. The states within the classical spinodal are thermodynamically unstable nonequilibrium states of a bulk system for which $\mathcal{F}_{LG}$ is the total free-energy functional. For a symmetric $A_{0.5}B_{0.5}$ alloy film considered earlier,[25] $\phi_o=0$. Many ϕ_o-dependent effects that emerge from our analysis do not occur for symmetric films. It is the Landau-Ginzburg free-energy term that is the source of many results obtained in this paper.

Linear elasticity is implicit in the expression for the elastic free-energy term, Eq. (11), which can be expressed either in terms of σ_{ij} and S_{ijkl} which are the elastic stress tensor and compliance tensor, respectively, or in terms of $u_{ij}\equiv\frac{1}{2}(\partial_j u_i+\partial_i u_j)$ and λ_{ijkl} which are the elastic strain tensor and elastic modulus tensor, respectively. Here u_i is the elastic displacement field and each of the subscripts i, j, k, or l can be x, y, or z. In the nonequilibrium process of growing alloy films, the mechanical equilibrium occurs on a time scale much faster than surface diffusion and we assume that it occurs instantaneously. By solving the equations of mechanical equilibrium, the **u** field can be obtained in terms of the other two fields $\delta\phi$ and δh, and in turn, the strain tensor field u_{ij} can be expressed as a function of $\delta\phi$ and δh. Elastic forces are long-range forces and the displacement field **u** at the top surface is dependent on **u** within the film and within the semi-infinite substrate. This dependence is seen explicitly through the equations of mechanical equilibrium and the boundary conditions at $z=-\infty$, $z=0$, and $z=h$. For a coherently growing film on a substrate, the elastic stress is proportional to the lattice mismatch $\epsilon=(a_f-a_s)/a_s$; if the film is an alloy, the stress also varies with (composition) fluctuation $\delta\phi$: $\sigma_{ij}\propto(\epsilon+\eta\delta\phi)$ where the solute-expansion coefficient $\eta=(\partial a_f/\partial\phi)/a_f$. The procedure of eliminating **u** in favor of $\delta\phi$ and δh has been described before by Huang and Desai[25] for symmetric alloy films and is the same for asymmetric films that we consider in this paper. We give an overview of this procedure and give the resulting expression for the displacement vector **u** within the film in Appendix A. For an elastically isotropic system, to which we restrict ourselves, $S_{ijkl}=\delta_{ik}\delta_{jl}(1+\nu)/E-\delta_{ij}\delta_{kl}\nu/E$ and $\lambda_{ijkl}=[E/(1+\nu)]\{\frac{1}{2}(\delta_{ik}\delta_{jl}+\delta_{il}\delta_{jk})+[\nu/(1-2\nu)]\delta_{ij}\delta_{kl}\}$ with Young's modulus E and Poisson ratio ν. Generally, the elastic constants of the film (denoted by a superscript f) depend on the local composition, and thus on mean order-parameter $\bar{\phi}$ (note $\bar{\phi}=\phi_o$) and on the order-parameter fluctuation $\delta\phi$. In the first-order approximation they are

$$E^f=E_o(\phi_o)(1+E_1^*\delta\phi),$$

$$\mu^f=\mu_o(\phi_o)(1+\mu_1^*\delta\phi), \tag{13}$$

where μ is the shear modulus and $\nu^f=(E^f/2\mu^f)-1\approx\nu_o$.

C. Equations of motion in Fourier space

For the asymmetric coherent alloy film, the surface free energy and elastic free energy terms make qualitative changes to the standard bulk alloy thermodynamics. Our goal in this paper is to analyze instabilities of the alloy film using a linear-stability analysis of the coupled kinetic Eqs. (5) and (6). The analysis is conveniently carried out using the two-dimensional Fourier components $\hat{h}(\mathbf{q},t)$ and $\hat{\phi}(\mathbf{q},z,t)$ which are defined as

$$\delta h(x,y,t)\equiv h-\bar{h}=\sum_{\mathbf{q}}\hat{h}(\mathbf{q},t)e^{i(q_xx+q_yy)}, \tag{14}$$

$$\delta\phi(x,y,z,t)\equiv\phi-\bar{\phi}=\sum_{\mathbf{q}}\hat{\phi}(\mathbf{q},z,t)e^{i(q_xx+q_yy)}. \tag{15}$$

For the linear-stability analysis, it is sufficient to obtain the detailed expressions for the three free-energy terms to second order in the fluctuations $\delta\phi$ and δh. The second-order expressions for $\mathcal{F}_s$ and $\mathcal{F}_{LG}$ can be directly obtained from Eqs. (9) and (10). The second-order expressions for $\mathcal{F}_{el}$ are given in Appendix B. Substitution of the second-order $\mathcal{F}$ in Eqs. (5) and (6) yields the coupled linearized dynamical equations, Eqs. (B13) and (B14), for the 2D Fourier components $\hat{h}(\mathbf{q},t)$ and $\hat{\phi}_s(\mathbf{q},t)\equiv\hat{\phi}(\mathbf{q},z=h,t)$. Here we rewrite these equations in terms of dimensionless variables. For this purpose we define $\ell_o=\gamma/E_o$ as a characteristic length and $\tau_o=\gamma^3/[(E_o)^4\Gamma_h]$ as a characteristic time. In terms of ℓ_o and τ_o, we define the dimensionless field variables $\hat{h}^*(\mathbf{k},\tau)=\hat{h}(\mathbf{q},t)/\ell_o$ and $\hat{\phi}_s^*(\mathbf{k},\tau)=\hat{\phi}_s(\mathbf{q},t)$, where $\mathbf{k}=\mathbf{q}\ell_o$ and $\tau=t/\tau_o$. The other quantities that enter the dimensionless equations are: $\sigma=\Omega\tau_o$, $V=v\tau_o/\ell_o$, $\zeta=\Gamma_\phi\ell_o/\Gamma_h\equiv\ell_o/\delta\equiv\ell_oN_v/N_s$, $r_e=r'/E_o$, $u_e=u/E_o$, $\kappa_e=\kappa E_o/\gamma^2$, $\chi=(1+\nu_o)/(1-\nu_o)$, $\alpha_o=[2E_1^*-(1+\nu_o)\mu_1^*]$, and $\beta_o=[8E_1^*-5(1+\nu_o)\mu_1^*]/[2(1-\nu_o)]$. Among these quantities, α_o and β_o depend on E_1^* and μ_1^* which arise from the dependence of the film elastic moduli on concentration fluctuations [see Eq. (13)]. The equations that $\hat{h}^*(\mathbf{k},\tau)$ and $\hat{\phi}_s^*(\mathbf{k},\tau)$ satisfy are

$$\frac{\partial\hat{h}^*}{\partial\tau}=a_{hh}\hat{h}^*+a_{h\phi}\hat{\phi}_s^*, \tag{16}$$

TABLE I. Material parameters: the Youngs modulus E, the lattice constant of alloy components a, the substrate lattice constant a_s, the surface-energy density of the film γ, and the Poisson Ratio ν_o. Parameters for Si-Ge/Si system (except ν_o) are from, Ref. 17, and for the other three systems from (Ref. 57) except as noted. Zincblende structure (Ref. 70) is assumed for GaN. Si, GaN, InN, and InP are, respectively, chosen to be component A in the Si-Ge, GaN-GaAs, InN-GaN, and InP-GaP alloys.

	Si-Ge/Si		GaAsN/GaAs		InGaN/GaN		InGaP/GaAs	
Physical constants	Si	Ge	GaN	GaAs	InN	GaN	InP	GaP
E ($\times 10^{11}$ J/m^3)	1.30	1.03	1.81	0.86	0.868[a]	1.81	0.611	1.03
a (10^{-10} m)	5.43	5.65	4.50	5.65	4.98[b]	4.50	5.87	5.45
a_s (10^{-10} m)	5.43 (Si)		5.65 (GaAs)		4.50 (GaN)		5.65 (GaAs)	
γ (J/m^2) [c]	2.51	1.93	4.1[a]	2.4[c]	2.2[a]	4.1[a]	1.8[c]	2.8[c]
ν_o	1/4	1/4	1/3	1/3	1/3	1/3	1/3	1/3

[a]Reference 71.
[b]Reference 72.
[c]Reference 73.

$$\frac{\partial \hat{\phi}_s^*}{\partial \tau} = a_{\phi h}\hat{h}^* + a_{\phi\phi}\hat{\phi}_s^*, \tag{17}$$

where

$$a_{hh} = k^3(2\chi\epsilon^2 - k), \tag{18}$$

$$a_{h\phi} = -k^2\left[(-r_e\phi_o + u_e\phi_o^3) + \frac{\alpha_o\epsilon^2}{(1-\nu_o)^2} + \frac{2\epsilon\eta}{(1-\nu_o)}\frac{\sigma - \nu_o kV}{\sigma + kV}\right], \tag{19}$$

$$a_{\phi h} = k^3\frac{2\zeta\chi\epsilon}{(1-\nu_o)}[(1-2\nu_o)\eta + \alpha_o\epsilon], \tag{20}$$

$$\begin{aligned} a_{\phi\phi} &= -V - \zeta k^2\left[\kappa_e k^2 - r_e + 3u_e\phi_o^2 + \frac{2\eta}{(1-\nu_o)}(\eta + \beta_o\epsilon)\right] \\ &\quad + \frac{Vk^3}{\sigma + kV}\frac{2\zeta\chi\eta}{(1-\nu_o)}[(1-2\nu_o)\eta + \alpha_o\epsilon] \\ &\equiv -V - \zeta k^2(\kappa_e k^2 + \mathcal{C}) + \frac{Vk^3}{\sigma + kV}F_1. \end{aligned} \tag{21}$$

Here we have defined

$$\mathcal{C} = -r_e + 3u_e\phi_o^2 + 2\eta(\eta + \beta_o\epsilon)/(1-\nu_o) \tag{22}$$

and

$$F_1 = 2\chi\zeta\eta[(1-2\nu_o)\eta + \alpha_o\epsilon]/(1-\nu_o). \tag{23}$$

An asymmetric alloy has a nonzero ϕ_o which introduces changes in $a_{h\phi}$ and $a_{\phi\phi}$. The dependence of $a_{h\phi}$ and $a_{\phi\phi}$ on σ arises from the Green's function $\hat{W}$ [Eqs. (A21) and (B7)] which is related to the long-range nature of the elastic forces and the mechanical equilibrium constraint. There is only an indirect dependence on ϕ_o in a_{hh} and $a_{\phi h}$ through the ϕ_o dependence of χ and ϵ.

D. Model parameters: T and ϕ_o dependences

We have applied the theory to four different alloy films: Si-Ge/Si, GaAsN/GaAs, InGaN/GaN, and InGaP/GaAs. For these four alloy systems,[69] we, respectively, denote Si, GaN, InN, and InP as component A and Ge, GaAs, GaN, and GaP as component B. In Table I, the Young's modulus E, lattice constant a, and surface tension γ are given for each of the alloy components for the four films. Also given is the substrate lattice constant a_s.

We use linear interpolation (Vegard's law[74])

$$a_f = [(a_A + a_B) + \phi_o(a_A - a_B)]/2, \tag{24}$$

and use the resulting $a_f(\phi_o)$ to obtain[75] $\eta = (a_A - a_B)/(2a_f)$ and $\epsilon = (a_f - a_s)/a_s$. We show the variation in ϵ and η with ϕ_o in Fig. 1. For InGaP film grown on GaAs substrate, ϵ changes from negative to positive values as ϕ_o varies from -1 (pure GaP) to $+1$ (pure InP) since the lattice constant for GaAs lies between those of GaP and InP; ϵ vanishes at $\phi_o = -0.0476$. Also since the lattice constants for GaAs and GaN are very different, ϵ for GaAsN becomes large and negative as ϕ_o approaches $+1$ (pure GaN). Experimentally it is difficult to incorporate more than a few percent[59] of GaN into GaAs.

For the ϕ_o dependence of γ and E_o, we also use a linear interpolation between their respective values at $\phi_o = -1$ and $+1$. We further assume a constant Poisson ratio ν_o with the result that $\mu_o = E_o/[2(1+\nu_o)]$ and $\mu_1^* = E_1^*$, where

$$E_1^*(\phi_o) = (E_A - E_B)/[2E_o(\phi_o)]. \tag{25}$$

The ϕ_o dependence of E_1^* and μ_1^* leads to the result that α_o and β_o also implicitly depend on ϕ_o.

As is evident, many of the parameters depend on ϕ_o and T. The ϕ_o dependence occurs for a_f, ϵ, η, N_v, N_s, E_o, γ, δ, ℓ_o, E_1^*, μ_1^*, α_o, β_o, ζ, r', r_e, u, u_e, κ, κ_e, Γ_h, and τ_o. Among these r', r_e, Γ_h, and τ_o also depend on T. In Table II, we give the parameters for symmetric alloy films, i.e., for $\phi_o = 0$. Except where indicated these values are taken from Ref. 57. The value of T used to obtain r', r_e, and τ_o for each of the four films is given in the caption.

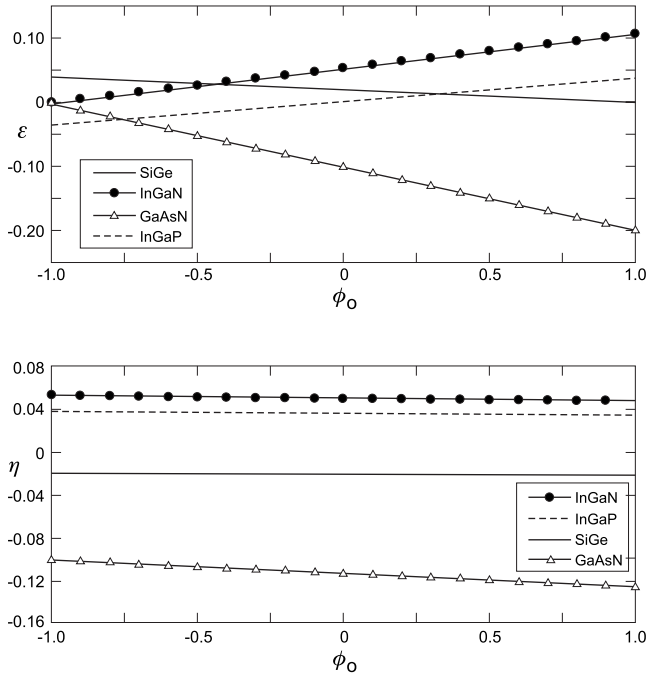

FIG. 1. Variation in lattice mismatch ϵ and solute expansion coefficient η with the composition ϕ_o. $\phi_o=1$ corresponds to the composition of pure component A which are Si, GaN, InN, and InP in Si-Ge, GaN-GaAs, InN-GaN, and InP-GaP alloy films, respectively. ϵ also depends on the substrate lattice constant a_s. The values of lattice constants of different components are given in Table I.

We show the temperature dependence of D_s and τ_o in Fig. 2. The kinetic coefficients Γ_ϕ and Γ_h depend on the surface-diffusion coefficient D_s. Among the various parameters that enter the theory, the temperature dependence of the surface diffusion coefficient D_s is the most sensitive, due to its Arrhenius behavior $D_s=D_o \exp(-E_g/k_BT)$ and is not accurately known in literature. This creates some uncertainty in numerical results. Fortunately, D_s enters the theory only though the characteristic time τ_o. The values of the prefactor D_o and activation energy E_g, that we use, are given[80] in Table II. In Fig. 2, τ_o is seen to change by 10–15 orders of magnitude as T is changed by a few hundred degrees. This dramatic variation is particularly relevant when comparing theory and experiment. In particular, an unstable system might appear stable on the experimental length and time scales.

III. LINEAR-STABILITY ANALYSIS

In Eqs. (16) and (17), we substitute $\hat{h}^*=h_o \exp(\sigma\tau)$ and $\hat{\phi}_s^*=\phi_{so} \exp(\sigma\tau)$. The latter is consistent with the substitution made to solve Eq. (A20) which resulted in Eq. (A21), since $\Omega t=\sigma\tau$. The substitution leads to

$$\begin{bmatrix} (\sigma - a_{hh}) & -a_{h\phi} \\ -a_{\phi h} & (\sigma - a_{\phi\phi}) \end{bmatrix} \begin{pmatrix} h_o \\ \phi_{so} \end{pmatrix} = 0, \tag{26}$$

which implies that the growth rate $\sigma(k)$ satisfies

$$[\sigma - a_{hh}(k)][\sigma - a_{\phi\phi}(k,\sigma)] - a_{h\phi}(k,\sigma)a_{\phi h}(k) = 0. \tag{27}$$

The regions of parameter space which lead to positive values of σ, as a result of solving Eq. (27), are regions of joint linear instability for both the fields $\hat{h}^*(k,\tau)$ and $\hat{\phi}_s^*(k,\tau)$. For the regions where $\sigma \leq 0$, linear-stability analysis implies either stability or metastability of the system.

A. Qualitative analysis

In order to get some qualitative idea of the solution of Eq. (27), set $\alpha_o=0$ and $\eta=0$ in Eqs. (18)–(21). This reduces Eq. (27) to

$$[\sigma - \sigma_o^{\rm lm}(k)][\sigma - \sigma_o^{\rm sd}(k)] = 0, \tag{28}$$

where

$$\sigma_o^{\rm lm}(k) = k^3(2\chi\epsilon^2 - k) \tag{29}$$

and

$$\sigma_o^{\rm sd}(k) = -V - \zeta k^2(-r_e + 3u_e\phi_o^2 + \kappa_e k^2). \tag{30}$$

$\sigma_o^{\rm lm}(k)$ is the root that leads the morphological instability, related to lattice mismatch (lm), for $0<k<2\chi\epsilon^2$; it reaches a maximum value of $\sigma_{max}^{\rm lm}(k_{max}^{\rm lm})=27(\chi\epsilon^2)^4/16$ at $k_{max}^{\rm lm}=3\chi\epsilon^2/2$. The other root, $\sigma_o^{\rm sd}(k)$, is related to the spinodal decomposition (sd) instability in which the deposition rate Λ plays a role through V. For $V>\zeta(-r_e+3u_e\phi_o^2)^2/(4\kappa_e)$, $\sigma_o^{\rm sd}(k)$ becomes a negative stable root and the system instability is driven by $\sigma_o^{\rm lm}(k)$.

For $V=0$, the static value of $\sigma_o^{\rm sd}$, $[\sigma_o^{\rm sd}]_{static}=\zeta k^2(r_e - 3u_e\phi_o^2 - \kappa_e k^2)$ is negative in the metastable region and positive in the spinodal region. The equation of the classical spinodal line separating the two regions is given by $r_e - 3u_e\phi_o^2=0$. The maximum value of $[\sigma_o^{\rm sd}]_{static}(k)$ is attained when $k=k_{max}^{\rm sd}=\sqrt{(r_e-3u_e\phi_o^2)/(2\kappa_e)}$ and is $\sigma_{max}^{\rm sd}(k_{max}^{\rm sd})=\zeta(-r_e + 3u_e\phi_o^2)^2/(4\kappa_e)$ which is also the cut-off value of V above which $\sigma_o^{\rm sd}(k)$ becomes negative.

The result that for very large V the largest positive root $\sigma_{max}(k)$ would approach $\sigma_o^{\rm lm}(k)$ is also true, in general. This can be seen as follows: (i) in the region of k where $\sigma_o^{\rm lm}$ is positive, $k\sim\chi\epsilon^2\sim 0.01$, since $\chi\sim 1$ and $\epsilon\sim 0.1$. (ii) $a_{hh}\sim\epsilon^8$, $a_{\phi\phi}\sim(-V)$, and $a_{\phi h}a_{h\phi}\sim\epsilon^{11}$ which makes it much smaller than $a_{hh}a_{\phi\phi}$. (iii) Neglecting $a_{\phi h}a_{h\phi}$ leads to two roots $a_{hh}=\sigma_o^{\rm lm}(k)$ and $a_{\phi\phi}\to(-V)$ provided $V\gg(\sigma/k)\sim k^3\sim(\chi\epsilon^2)^3\sim 10^{-6}$.

For the general case, one cannot set $\alpha_o=0$ or $\eta=0$, and the general solution arises from the coupling of the two instabilities due to nonzero η and α_o. We first consider the solutions of Eq. (27) in certain limiting cases before discussing the general case.

B. One component film

If only a single component is deposited on a substrate (e.g., Ge on Si), only the height field $\hat{h}^*$ is relevant. The detailed analysis has been done by Spencer *et al.*[4] One has $\hat{h}^*=h_o \exp(\sigma\tau)$ with $\sigma=a_{hh}(k)=\sigma_o^{\rm lm}(k)=k^3(2\chi\epsilon^2-k)$ where the first term arising from the lattice mismatch ϵ is always

TABLE II. Material parameters related to the LG and elastic-free energies for a symmetric mixture, $\phi_o=0$. For example, the values of γ and E_o for the film are given, for a symmetric mixture, as the mean of the respective component values given in Table I. Many parameters in this table depend on ϕ_o. The parameters r', r_e, and τ_o also depend on temperature T for which the values used are 200 K for Si-Ge/Si, 500 K for GaAsN/GaAs, 800 K for InGaN/GaN, and 823 K for InGaP/GaAs. Si, GaN, InN, and InP are, respectively, chosen to be the component A in Si-Ge, GaN-GaAs, InN-GaN, and InP-GaP alloy films.

Parameters	Si-Ge/Si[a]	GaAsN/GaAs	InGaN/GaN	InGaP/GaAs
$\chi_r(10^4$ J/mole)	0.43	21.6[b]	2.99	2.08
T_c(K)	261	13000	1800[c]	1250[d]
$E_o(10^{11}$ J/m^3)	1.17	1.34	1.34	0.821
γ(J/m^2)	2.22	3.25	3.15	2.3
$a_f(10^{-9}$ m)	0.554	0.508	0.474	0.566
$\delta(10^{-9}$ m)	0.139	0.254	0.237	0.283
$\ell_o(10^{-11}$ m)	1.9	2.43	2.35	2.8
$r'(10^8$ J/m^3)	0.39	52.5	5.18	1.3
r_e	0.000339	0.0393	0.00387	0.00159
$u(10^8$ J/m^3)	0.564	18.2	3.11	1.27
u_e	0.000484	0.0136	0.00232	0.00155
$\kappa(10^{-10}$ J/m)	0.016	1.77	0.26	0.15
κ_e	0.0385	2.24	0.354	0.236
E_1^*	0.116	0.356	−0.352	0.255
μ_1^*	0.116	0.356	−0.352	0.255
α_o	0.087	0.237	−0.235	0.17
β_o	0.135	0.356	−0.352	0.255
ζ	0.137	0.0958	0.0993	0.0991
D_o(m^2/s)	8.45×10^{-10}	2.5×10^{-6}	1.21×10^{-5}	1.6×10^{-5}
E_g(eV)	0.83	1.5[e]	1.0	1.2
τ_o(s)	5.2×10^4	5.85×10^{-6}	2.81×10^{-14}	3.28×10^{-13}

[a]Reference 17.
[b]Reference 61.
[c]References 76 and 77.
[d]References 30 and 78.
[e]Reference 79.

destabilizing regardless of the sign of ϵ and the second term originating from the surface energy is always stabilizing. The growing film is unstable for $0<k<k_c\equiv 2\chi\epsilon^2$. The maximal instability occurs at $k_m=3k_c/4$ with $\sigma(k_m)=27\chi^4\epsilon^8/16$. The peak of the instability moves to longer wavelengths as ϵ is decreased. The critical thickness of the film, defined as $h_c\equiv\ell_c/\ell_o=V/\sigma(k_m)$, depends steeply on ϵ as ϵ^{-8}.

C. Limit $\epsilon=0$

This limit corresponds to growth of a film on a lattice-matched substrate, such that $\epsilon=0$. For InGaP films grown on a GaAs substrate, ϵ vanishes at $\phi_o=-0.0476$ corresponding to about 48% InP in the alloy film. In $\epsilon=0$ limit $a_{hh}=-k^4$, $a_{h\phi}=-k^2(-r_e\phi_o+u_e\phi_o^3)$, $a_{\phi h}=0$, and $a_{\phi\phi}=-V-\zeta k^2(-r_e+3u_e\phi_o^2+\frac{2\eta^2}{(1-\nu_o)}+\kappa_e k^2)+\frac{Vk^3}{\sigma+kV}\frac{2\zeta\chi\eta^2(1-2\nu_o)}{(1-\nu_o)}$. The characteristic equation then takes the form

$$(\sigma+k^4)(\sigma^2+a_1\sigma+a_0)=0, \tag{31}$$

where

$$a_1=\left[(1+k)V+\zeta k^2\left(-r_e+3u_e\phi_o^2+\frac{2\eta^2}{(1-\nu_o)}+\kappa_e k^2\right)\right] \tag{32}$$

and

$$a_0=kV\left[V+\zeta k^2\left(-r_e+3u_e\phi_o^2+\frac{4\eta^2\nu_o^2}{(1-\nu_o)^2}+\kappa_e k^2\right)\right]. \tag{33}$$

For dynamically growing films the linear instability/stability of the film is governed by Eq. (31), where the root $\sigma=-k^4$ is a stable root. The instability, if any, will arise if either of the two roots of the remaining quadratic becomes positive. The two remaining roots, expressed as $\sigma_\pm=[-a_1\pm\sqrt{a_1^2-4a_0}]/2$, can be explicitly written as

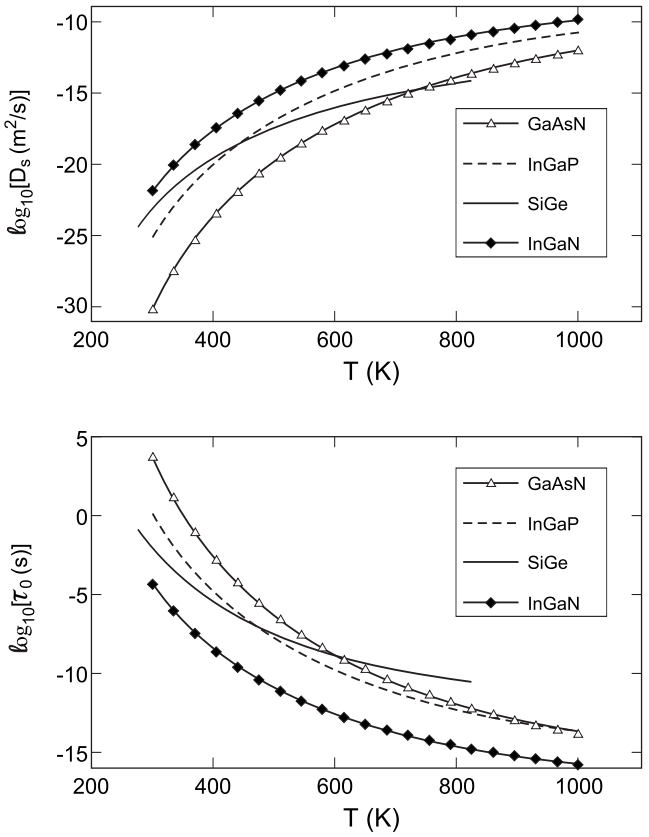

FIG. 2. The surface-diffusion constant D_s and the characteristic unit of time τ_o follow an Arrhenius dependence on temperature T, and depend on the binding energy E_g and prefactor D_o. D_o and E_g are given in Table II. τ_o changes over many orders of magnitude on changing T by a few hundred degrees.

$$\sigma_{\pm} = \frac{1}{2}[(\sigma_1^0 + \sigma_3^0) \pm \sqrt{(\sigma_1^0 - \sigma_3^0)^2 + 8(1+\nu_o)(1-2\nu_o)\zeta\eta^2 V k^3/(1-\nu_o)^2}], \tag{34}$$

where $\sigma_1^0 = -kV$ and $\sigma_3^0 = -V - \zeta k^2(-r_e + 3u_e\phi_o^2 + \frac{2\eta^2}{(1-\nu_o)} + \kappa_e k^2)$. In case of instability, the k variation in the largest positive root can be tracked: at some value of k, denoted by k_{max}, the positive root will have its maximum value, denoted as σ_{max}. The variation in k_{max} and σ_{max} with V at different values of T gives a quantitative measure of the instability. Figure 3 shows σ_{max} as a function of V for various T for InGaP/GaAs at $\phi_o = -0.0476$, $\epsilon = 0$. As T increases, the range of V, for which the instability occurs, decreases. For $T \geq 900$ K, no instability is found. For each positive value of σ_{max}, the corresponding $k_{max} = 0.0001$. For values of V outside the range of positive σ_{max}, σ_{max}, and k_{max} vanish, indicating stability.

In general, the condition for stability requires $a_1 > 0$ and $a_0 > 0$. Now if $2\eta^2/(1-\nu_o) > r_e$, then $a_1 > 0$ is satisfied. The condition $a_0 > 0$ for any k gives the constraint on V that $V > V_o$, where $V_o = \zeta[-r_e + 3u_e\phi_o^2 + 4\eta^2\nu_o^2/(1-\nu_o)^2]^2/(4\kappa_e)$. For $V < V_o$, the alloy film is linearly unstable to segregation due to the coupling of η with the growth velocity V. However, if in a_0, the combination $[-r_e + 3u_e\phi_o^2 + 4\eta^2\nu_o^2/(1-\nu_o)^2] > 0$, then the film is stable irrespective of the value of V.

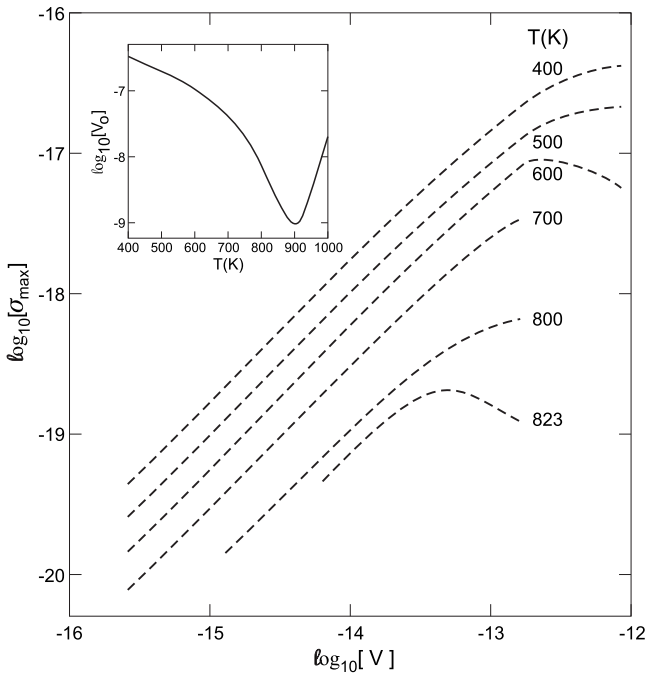

FIG. 3. Unstable root for InGaP/GaAs at $\phi_o = -0.0476$, $\epsilon = 0$. σ_{max} as a function of V shown for various T in a double-logarithmic plot. For each positive σ_{max} value, the corresponding $k_{max} = 0.0001$. σ_{max} and k_{max} vanish for V values outside the range shown for each T, indicating stability. The inset shows $\log_{10}[V_o]$ as a function of T.

If for $2\eta^2/(1-\nu_o) < r_e$, in a_1, the combination $[-r_e + 3u_e\phi_o^2 + 2\eta^2/(1-\nu_o)] < 0$, then the condition for stability, resulting from $a_1 > 0$, has to be explored numerically. The other condition, emerging from $a_0 > 0$, remains the same: $V > V_o$.

The inset in Fig. 3 shows V_o as a function of T for InGaP/GaAs at $\phi_o = -0.0476$, $\epsilon = 0$. The range of V where instability is found is at least three orders of magnitude smaller than V_o.

D. Static limit

The static films correspond to $V = 0$ limit. In this limit $a_{\phi\phi}$ and $a_{h\phi}$ become independent of σ and Eq. (27) becomes a quadratic equation in σ

$$\sigma^2 + A_1\sigma + A_0 = 0, \tag{35}$$

where the coefficients $A_1 = -\lim_{V\to 0}(a_{hh} + a_{\phi\phi})$ and $A_0 = \lim_{V\to 0}(a_{hh}a_{\phi\phi} - a_{\phi h}a_{h\phi})$ can be easily obtained from Eqs. (18)–(21). Again, the condition for stability requires that $A_1 > 0$ and $A_0 > 0$. At $k = 0$, both A_0 and A_1 vanish with the consequence that both the roots vanish. In the parameter space, the surface between unstable and stable regions is the surface defined by $A_0 = 0$ since one of the roots vanishes on this surface. The marginal stability on this surface also requires that the other nonzero root be negative which additionally requires $A_1 \geq 0$. The stability conditions $A_1 > 0$ and $A_0 > 0$ for the entire range of k reduces to the following four inequalities:

$$\mathcal{C} > 0, \tag{36}$$

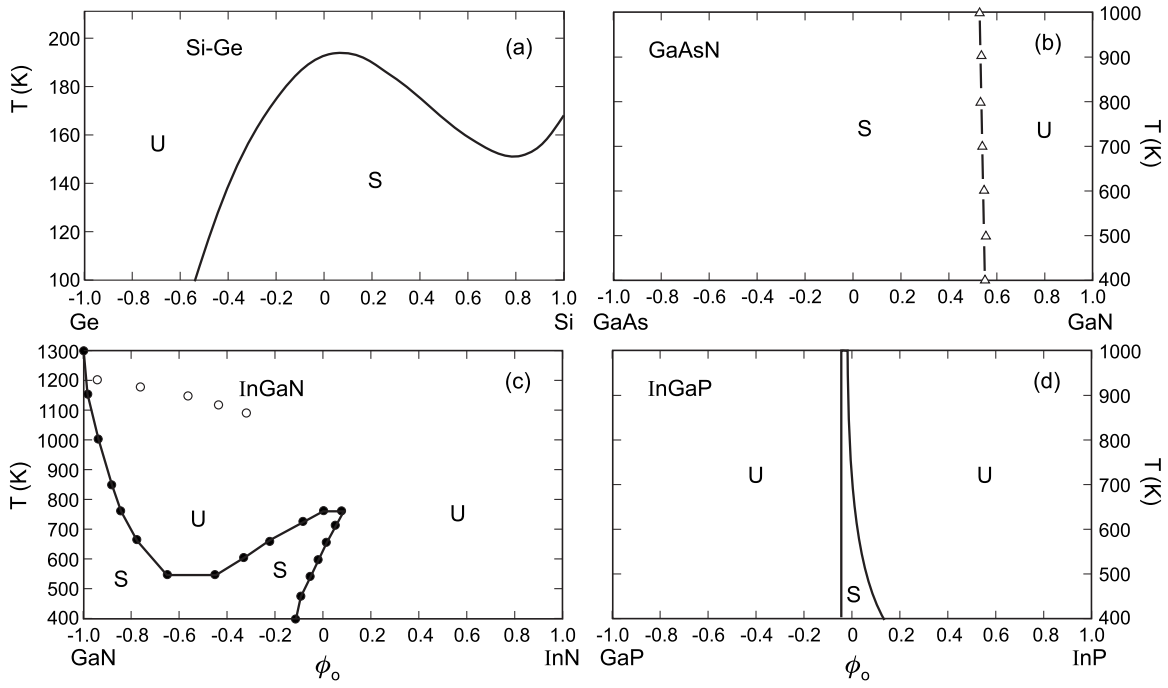

FIG. 4. The regions of stability (S) and instability (U) in the (T-ϕ_o) plane for $V=0$ (static film limit): (a) Si-Ge/Si film, (b)GaAsN/GaAs film, (c) InGaN/GaN film, and (d) InGaP/GaAs film. The open circles in (c) correspond to (T-ϕ_o) points where instability has been observed for InGaN/GaN by Rao *et al.* (Ref. 38).

$$\zeta\mathcal{C} - \frac{(\chi\epsilon^2)^2}{(1+\zeta\kappa_e)} > 0, \tag{37}$$

$$-2\chi\epsilon^2\zeta\mathcal{C} + P > 0, \tag{38}$$

where

$$P = \frac{2\chi\zeta\epsilon}{(1-\nu_o)}[(1-2\nu_o)\eta + \alpha_o\epsilon] \times\left\{\frac{\alpha_o\epsilon^2}{(1-\nu_o)^2} + \frac{2\epsilon\eta}{(1-\nu_o)} - r_e\phi_o + u_e\phi_o^3\right\}. \tag{39}$$

Also if $(4m^2-3\kappa_e\mathcal{C})>0$, where $m=\kappa_e\chi\epsilon^2$, then an extra condition needs to be satisfied

$$-2\zeta\{18\mathcal{C}\kappa_e m + 8m^3 + (4m^2-3\kappa_e\mathcal{C})^{3/2}\} + 27\kappa_e^2 P > 0. \tag{40}$$

Here $\mathcal{C}$ is given by Eq. (22). For $\epsilon=0$, the boundary of the unstable region is given by Eq. (36), which is also the spinodal curve.[8] However, for $\epsilon\neq 0$, the other three inequalities in Eqs. (37), (38), and (40) contribute to instability. For low values of ϵ the boundaries of the unstable region then extend to include regions on either side of the spinodal curve. This implies that ϵ has a dominant role in turning the regions which are metastable due to phase-segregation phenomena into unstable regions.

While some of the material parameters that enter the four inequalities in Eqs. (36)–(38) and (40) are constant, many depend on ϕ_o and r_e depends on both ϕ_o and T. Once ϕ_o and T are chosen, it is straightforward to calculate the left-hand side of each of the inequalities and, in turn, determine whether the static film is stable, marginally stable or unstable at that point in the ϕ_o-T plane. In the calculations, full ϕ_o and T dependences are included. The stability results are shown in Fig. 4: the stability boundaries for Si-Ge/Si film in (a), GaAsN/GaAs film in (b), InGaN/GaN film in (c), and for InGaP/GaAs film in (d). For GaAsN/GaAs and Si-Ge/Si films, it is the inequality in Eq. (38) that is violated in the unstable regions. For the InGaN/GaN film, however, one or more of all the four inequalities are violated depending on ϕ_o and T. The open circles in (c) correspond to (T-ϕ_o) points where instability has been observed for InGaN/GaN by Rao *et al.*[38] The InGaP/GaAs film is stable only in a rather narrow range of ϕ_o within the region $400<T<1000$ K due to the violation of the inequality in Eq. (38); the left edge of the stable region is at $\phi_o=-0.0476$; at this value of ϕ_o, $\epsilon=0$.

Within the unstable regions, the positive roots of the quadratic Eq. (35) lead to growth of fluctuations. The roots of this quadratic are

$$\sigma_\pm = -\frac{1}{2}k^2[(1+\zeta\kappa_e)k^2 - 2\chi\epsilon^2 k + \zeta\mathcal{C}] \pm \frac{1}{2}k^2\sqrt{\{(1-\zeta\kappa_e)^2k^4 - 4\chi\epsilon^2(1-\zeta\kappa_e)k^3 + 4[(\chi\epsilon^2)^2 - \zeta\mathcal{C}]k^2 - 4(P-\zeta\mathcal{C}\chi\epsilon^2)k + (\zeta\mathcal{C})^2\}}. \tag{41}$$

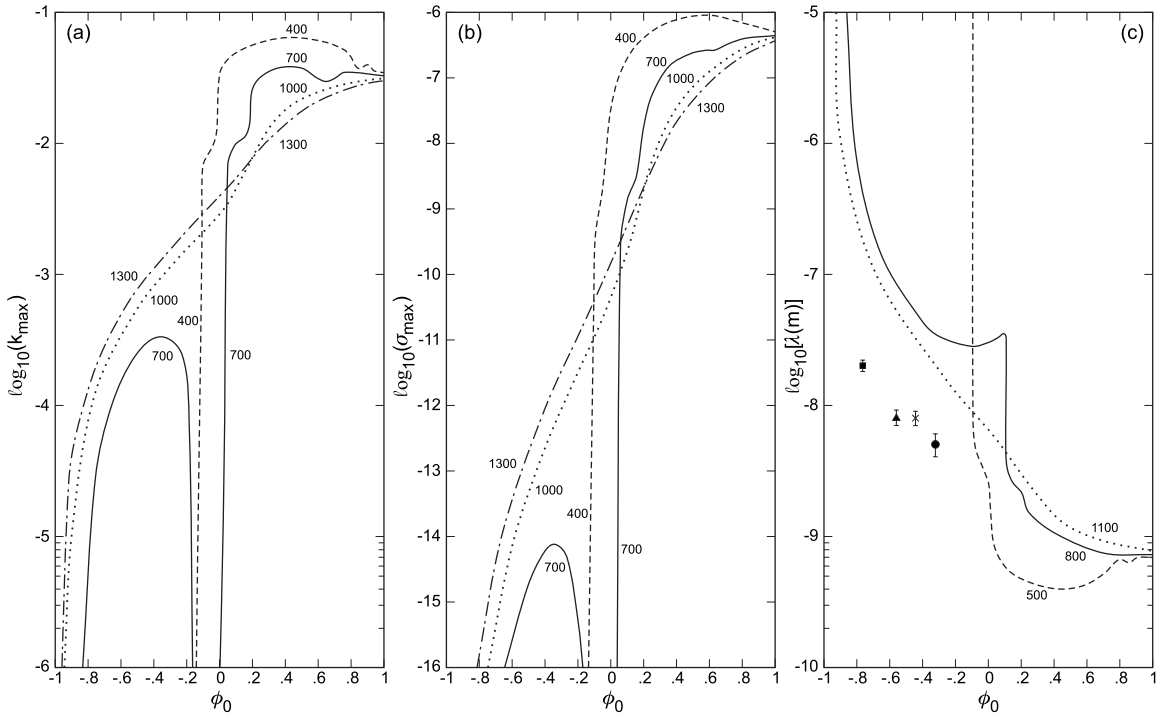

FIG. 5. InGaN/GaN film: the ϕ_o variation in (a) k_{max}, (b) σ_{max}, and (c) λ(m) for various T. In (c), the experimental results of Rao *et al.* (Ref. 38) are shown: $[T(\mathrm{K}), \phi_o] = (1093, -0.32)$—solid circle; $(1123, -0.44)$—cross; $(1153, -0.56)$—solid triangle; and $(1183, -0.76)$—solid square at $(1200, -0.94)$ $\lambda = \infty$.

This result is used to analyze static alloy films in the unstable region for the case of zinc-blende InGaN/GaN film. Again by tracking k variation in $\sigma_{\pm}$, the maximally unstable mode at (k_{max}, σ_{max}) can be obtained in the unstable region of the (T, ϕ_o) plane. This mode diverges exponentially with time and outgrows all other growing modes in a linear-stability analysis. The corresponding wavelength of the fluctuations is $\lambda \simeq \ell_o / k_{max}$. In Fig. 5, we show the results for a InGaN/GaN film: k_{max}, σ_{max}, and λ(m) are shown as functions of ϕ_o for various T. The experimental results by Rao *et al.*[38] for λ(m) at four different $[T(\mathrm{K}), \phi_o]$ points are also shown. The comparison has to be looked at with some caution. The theory is applicable only to zinc-blende systems since a cubic symmetry of the substrate and the coherent film is implicit in the theory; the experiments are, however, for a wurtzite case with a hexagonal symmetry; the comparison is done just to show that the trend of the ϕ_o variation is similar: λ increases as ϕ_o decreases and reaches ∞ at the unstable/stable boundary.

E. General case

The general case corresponds to the solution of Eq. (27) for $\sigma(k)$. Since the expressions for both $a_{\phi\phi}$ [Eq. (21)] and $a_{h\phi}$ [Eq. (19)] contain $(\sigma + kV)$ in a denominator, we rationalize Eq. (27) by multiplying it with $(\sigma + kV)$ to obtain a cubic equation for $\sigma(k)$

$$\sigma^3 + a_2(k)\sigma^2 + a_1(k)\sigma + a_0(k) = 0, \tag{42}$$

where

$$a_2(k) = (1+k)V + k^2\zeta\mathcal{C} - k^3 2\chi\epsilon^2 + k^4(\zeta\kappa_e + 1),$$

$$= -(-kV + \sigma^{\mathrm{lm}} + \sigma^{\mathrm{sd}}), \tag{43}$$

$$a_1(k) = kV^2 + k^3V(\zeta\mathcal{C} - F_1 - 2\chi\epsilon^2) + k^4V(1 - 2\chi\epsilon^2) + k^5[V(\zeta\kappa_e + 1) + P - 2\chi\epsilon^2\zeta\mathcal{C}] + k^6\zeta\mathcal{C} - k^7 2\chi\epsilon^2\zeta\kappa_e + k^8\zeta\kappa_e,$$

$$= \sigma^{\mathrm{lm}}\sigma^{\mathrm{sd}} - kV(\sigma^{\mathrm{lm}} + \sigma^{\mathrm{sd}}) - k^3VF_1 + k^5P, \tag{44}$$

and

$$a_0(k) = -k^4V^2 2\chi\epsilon^2 + k^5V^2 + k^6V(P - 2\chi\epsilon^2\zeta\mathcal{C}) + k^7V(\zeta\mathcal{C} - F_1) - k^8V2\chi\epsilon^2\zeta\kappa_e + k^9V\zeta\kappa_e,$$

$$= kV\sigma^{\mathrm{lm}}\sigma^{\mathrm{sd}} + k^6VP - k^7VF_1. \tag{45}$$

Here $\sigma^{\mathrm{lm}} \equiv \sigma_o^{\mathrm{lm}}$ is given in Eq. (29), and $\mathcal{C}$, F_1, and P are given, respectively, in Eqs. (22), (23), and (39). Also

$$\sigma^{\mathrm{sd}} = -V - k^2\zeta(\mathcal{C} + k^2\kappa_e) \equiv \sigma_o^{\mathrm{sd}} - k^2\zeta[2\eta(\eta + \beta_o\epsilon)/(1 - \nu_o)]. \tag{46}$$

If, in each of $a_1(k)$ and $a_0(k)$, the terms proportional to P and to F_1 are ignored, then the cubic equation reduces to

$$(\sigma + kV)(\sigma - \sigma^{\mathrm{lm}})(\sigma - \sigma^{\mathrm{sd}}) = 0. \tag{47}$$

The root $(-kV)$ is associated with a stable growth due to deposition in absence of fluctuations and diffusion, and the other two, σ^{lm} and σ^{sd}, represent two decoupled instabilities. The coupling arises from the terms proportional to P and F_1. When these terms are included, it is not possible to obtain

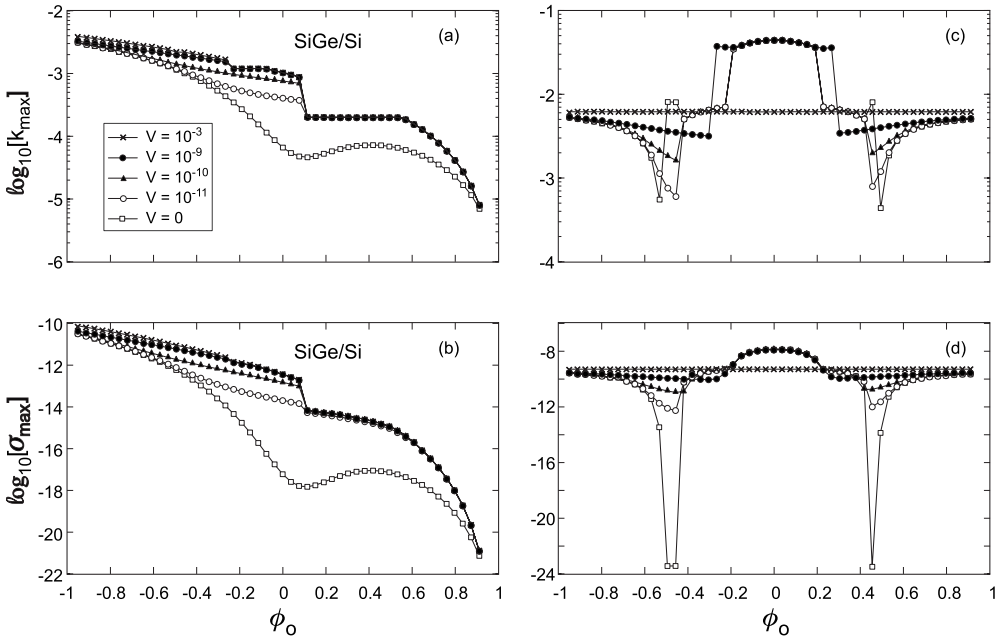

FIG. 6. k_{max} and σ_{max} as functions of ϕ_o at $T=200$ K for different values of growth velocity V [see legend box in (a)]. Left half [(a) and (b)] for ϕ_o-dependent parameters appropriate to Si-Ge/Si films. Right half [(c) and (d)] the same except η is held fixed at +0.005 and ϵ at +0.05.

simple analytic expressions for the roots of the cubic. If the term proportional to F_1 is ignored in each of $a_1(k)$ and $a_0(k)$, analytic expressions for the coupled roots can be obtained. The root $(-kV)$ remains unchanged and the other two roots are

$$\sigma_2^{approx} = \sigma^{\rm lm} - \Delta,$$

$$\sigma_3^{approx} = \sigma^{\rm sd} + \Delta,$$

where

$$\Delta = \frac{1}{2}[-(\sigma^{\rm sd} - \sigma^{\rm lm}) + \sqrt{(\sigma^{\rm sd} - \sigma^{\rm lm})^2 - 4k^5 P}]. \qquad (48)$$

However, ignoring the terms proportional to F_1 is rarely justified, and to proceed further, the analysis for the general case requires numerical approach. The goal in the numerical analysis is to probe the stability/instability of a system in the (V,T,ϕ_o) space through the exact numerical roots σ_1, σ_2, and σ_3 of the cubic characteristic equation. For each chosen point (V,T,ϕ_o), various parameters can be uniquely obtained and the three roots of the cubic can be obtained as functions of k. If any one (or more) of the three roots is positive for a range of k values, one can uniquely obtain the maximum root σ_{max} and the associated k value, (k_{max}) at which this maximum occurs. When the system is unstable, the growth of the fluctuations is dominated by the value of the (real part of the) maximum, $\sigma_{max}(k_{max})$. This mode diverges exponentially with time and outgrows all other growing modes. The corresponding wavelength of the fluctuations is $\lambda \simeq \ell_o/k_{max}$.

The variation in numerical roots σ_1, σ_2, and σ_3 with k contains the richness and complexity of Eqs. (42)–(45). The coupling of the two instabilities, arising from nonzero F_1 and P, often leads to two positive roots, say, σ_2 and σ_3; as k increases, occasionally these two merge into a complex pair $(\sigma_{re} \pm i\sigma_{im})$ with $\sigma_{re} > 0$ (oscillatory instability). The goal of the numerical analysis is to map out the (real part of the) maximally unstable root $\sigma_{max}(k_{max})$ in the parameter space of T, V, and ϕ_o. The most unstable root $\sigma_{max}(k_{max})$ often switches from one of the positive roots, say, σ_2, to another, say, σ_3, as the analysis moves in the (T,V,ϕ_o) space. Many of the parameters depend on ϕ_o and T. The ϕ_o dependence occurs for a_f, ϵ, η, N_v, N_s, δ, E_o, γ, E_1^*, μ_1^*, α_o, β_o, r_e, u_e, κ_e, ℓ_o, τ_o, ζ, and Γ_h. Among these r_e, Γ_h, and τ_o also depend on T; Γ_h and τ_o vary rapidly with T due to their dependence on D_s which has an Arrhenius behavior (Fig. 2). Figure 6 illustrates the sensitivity of results on the ϕ_o and T dependences of the parameters and indicates the importance of fully including them in the analysis.

Figure 6 shows the variation in k_{max} and σ_{max} with ϕ_o for various values of V. The left half [(a) and (b)] shows the results for the Si-Ge/Si film where $T=200$ K and the ϕ_o variation in all the parameters is fully included. From Fig. 1 one has η nearly independent of ϕ_o with a value of −0.02 and ϵ varying linearly between +0.04 and 0 as ϕ_o changes from −1 to +1. In the right half [(c) and (d)], η is held fixed at +0.005 and ϵ at +0.05 while the remaining parameters kept with ϕ_o variation as in the left half. The choice of $T=200$ K is made in order to have $T < T_c$. In the right half, a larger value of ϵ and a rather small positive value of η are chosen to enhance effects of lattice mismatch. For $V=10^{-3}$, in the right half, σ^{max} is independent of ϕ_o and has a value of $\sim 5.1\times 10^{-10}$ which is comparable to $\sigma_{max}^{\rm lm} = 27\chi^4\epsilon^8/16$. This is the expected behavior for large V. The corresponding $k_{max} = 3\chi\epsilon^2/2 = 6.25\times 10^{-3}$ corresponds to the instability wavelength of $2\pi\ell_o/k^{max} \sim 1.9\times 10^{-8}$ m. The growth rate $\sigma^{max} \sim 5.1\times 10^{-10}$ corresponds to a rather large evolution time scale of $\tau_o/\sigma^{max} \sim 10^{16}$ s, but there is some uncertainty

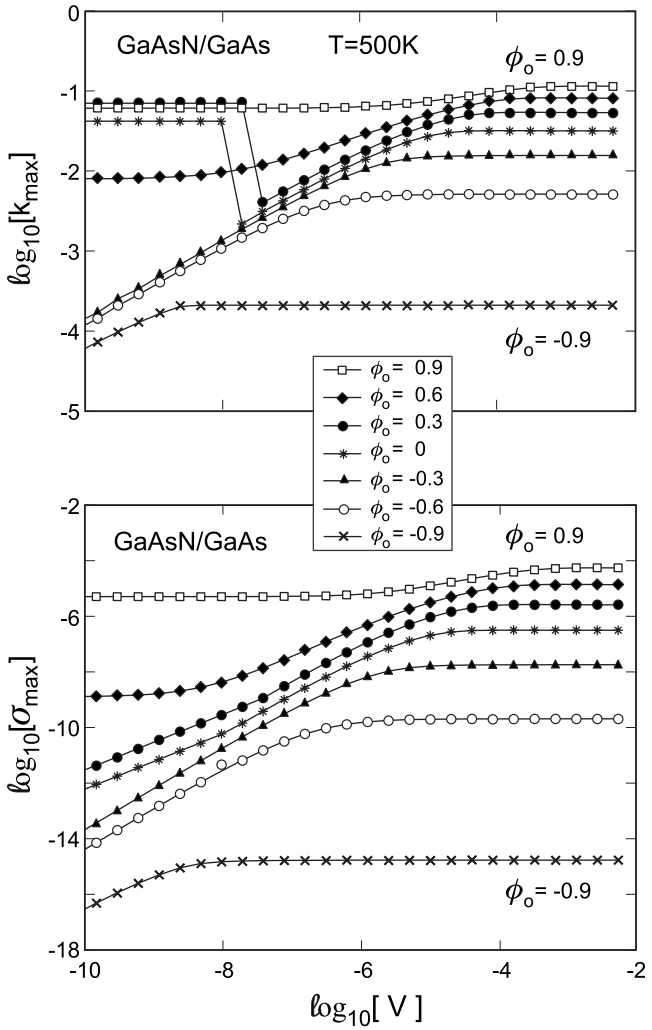

FIG. 7. GaAsN/GaAs films: k_{max} and σ_{max} vs V, at $T=500$ K, for various values of ϕ_o. From top to bottom, $\phi_o=0.9$ (squares), 0.6 (solid diamonds), 0.3 (solid circles), 0 (asterisks), −0.3 (solid triangles), −0.6 (open circles), and −0.9 (crosses).

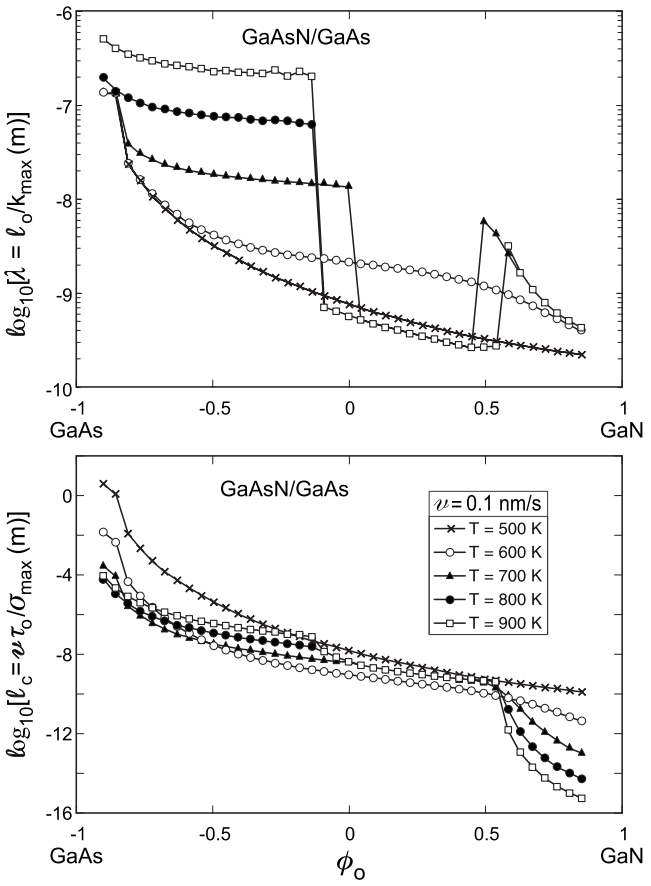

FIG. 8. GaAsN/GaAs films: λ and ℓ_c vs ϕ_o at various values of T as shown. The growth velocity is fixed at $\upsilon=0.1$ nm s^{-1}.

in τ_o due to uncertainty in D_s. In the left half, where the linear ϕ_o variation in ϵ is retained, for $V=10^{-3}$, the ϵ^2 behavior for $k_{max}\to\phi_o^2$ behavior and a much steeper ϵ^8 behavior for $\sigma_{max}\to\phi_o^8$ is not yet fully achieved; a larger V is needed for the $\sigma_{max}^{\rm Im}$ to dominate. In the next section, we fully include the (ϕ_o,T) dependences of all the parameters and apply the theory to alloy films of III-V group whose material parameters at each pair (ϕ_o,T) can be obtained using those given in Tables I and II.

IV. APPLICATION TO GROUP III-V FILMS

A. Nitride films: GaAsN/GaAs and InGaN/GaN

In Fig. 7, k_{max} and σ_{max} are shown as functions of V for various values of ϕ_o at $T=500$ K. For large values of V, k_{max} equals $3\chi[\epsilon(\phi_o)]^2/2$ and σ_{max} equals $27(\chi[\epsilon(\phi_o)]^2)^4/16$ as expected. For a fixed, large value of V, as ϕ_o increases, the magnitude of $\epsilon(\phi_o)$ increases (see Fig. 1). This leads to an increase in both $[\epsilon(\phi_o)]^2$ and $[\epsilon(\phi_o)]^8$, which results in the monotonic upward shift of the $k_{max}(V)$ and $\sigma_{max}(V)$ curves on the large V side.

The jump in value of k_{max} for $\phi_o=0.3$ and $\phi_o=0$ around $V=10^{-8}$ corresponds to a switch between maxima of two different roots of the cubic, Eq. (42). Specifically, at large values of V (flat horizontal portion of the curve in Fig. 7), k_{max} and σ_{max} are dominated by the morphological instability arising from lattice mismatch. As V is decreased, this root gets gradually more coupled with the spinodal decomposition instability leading to a gradual decrease in k_{max} and σ_{max} until around $V\sim10^{-7}$–10^{-8}, at which point a discontinuous jump occurs in k_{max} to a different root with a higher k_{max} but the same σ_{max}. In this region the two instabilities are strongly coupled. (Since σ_{max} value does not change during the switch among two roots, there is no jump discontinuity in the bottom half of Fig. 7.) A similar phenomena is seen also in results for other films which are shown below.

The results displayed in Fig. 7 are in terms of dimensionless quantities. It is useful to show them in a different way using dimensional quantities. This is done in Fig. 8. Its top half shows the wavelength (in meters) of the maximally growing Fourier component of fluctuations $\lambda=\ell_o/k_{max}$ as a function of ϕ_o for various temperatures (see legend in bottom half). A part of the top half is enlarged in Fig. 9. The region enlarged has $-0.95<\phi_o<-0.90$ and $T=673$ and 723 K. The two solid points correspond to two films experimentally grown by McGee *et al.*[63] [see Table I, Figs. 4(a) and

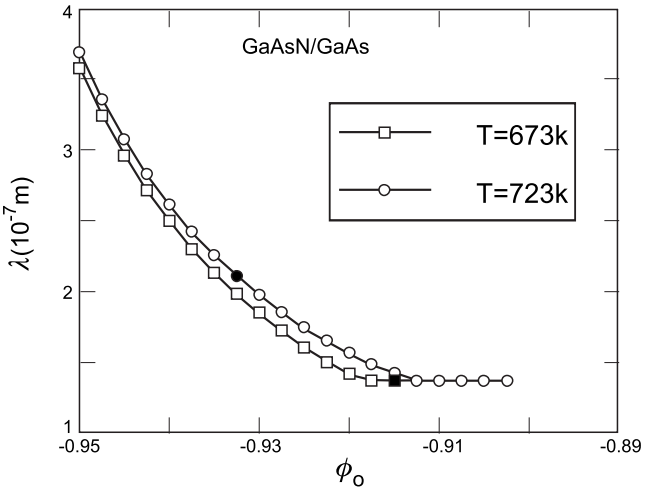

FIG. 9. GaAsN/GaAs films: λ vs ϕ_o at $T=673$ and 723 K and comparison with films grown by McGee *et al.* (Ref. 63) The growth velocity is fixed at $v=0.1$ nm s^{-1}.

4(b) in this paper]. The two experimentally grown films correspond to [$T=673$ K, $x=0.042$, and $\phi_o=-0.916$ (solid square)] and [$T=823$ K, $x=0.034$, and $\phi_o=-0.932$ (solid circle)], respectively. In agreement with experimental observation, the wavelength λ increases with T, however, the significant reason for this increase is a combination of both the decrease in ϕ_o or equivalently in x, and the increase in T.

The bottom half of Fig. 8 shows the critical thickness ℓ_c which is defined in the following manner. The Fourier component of the maximally growing fluctuation of the film height behaves as $\hat{h}^*=h_o \exp(\sigma_{max}\tau)$; until time τ_c defined as $\sigma_{max}\tau_c=1$, the exponentially growing fluctuations are reasonably contained; the mean height of the film at time τ_c is referred to as the critical film thickness ℓ_c. Thus, in meters, $\ell_c=v\tau_o\tau_c=v\tau_o/\sigma_{max}=V\ell_o/\sigma_{max}$. For film thickness smaller than ℓ_c, one expects, even for unstable films, a nearly flat top surface as the film grows. We have chosen a typical value of growth velocity: $v=0.1$ nm s^{-1}. When v is fixed, for a given T, the dimensionless growth velocity V remains approximately constant as ϕ_o changes from −1 to +1. However V depends strongly on T: for the results shown in the bottom half of Fig. 8, $V\simeq 2\times10^{-4}$, 10^{-6}, 2×10^{-8}, 8×10^{-10}, and 8×10^{-11} for $T=500$, 600, 700, 800, and 900 K, respectively. For $v=0.1$ nm s^{-1}, the bottom half of Fig. 8 shows that for small N content in a GaAsN film, say, $x=0.1$ or equivalently $\phi_o=-0.8$, the critical thickness is at least[81] 100 nm at each of the five T values. Higher the temperature, lower is the value of ℓ_c above which the top film surface begins to roughen. Also, for a given T, higher the ϕ_o (equivalently higher the x of N), greater the instability of the film and lower the value of ℓ_c. Note that discontinuities in k_{max} show up as discontinuities in λ and lack of discontinuities in σ_{max} results in a similar lack in ℓ_c.

Figure 10 shows the variation in k_{max} and σ_{max} with V for an InGaN/GaN film at 800 K for various values of ϕ_o. In Fig. 11, the variation in λ and ℓ_c with ϕ_o is shown for various T at fixed growth velocity $v=0.1$ nm s^{-1}. These results are qualitatively similar to those for a GaAsN/GaAs film. Again, for a fixed T, V is approximately constant as ϕ_o is varied:

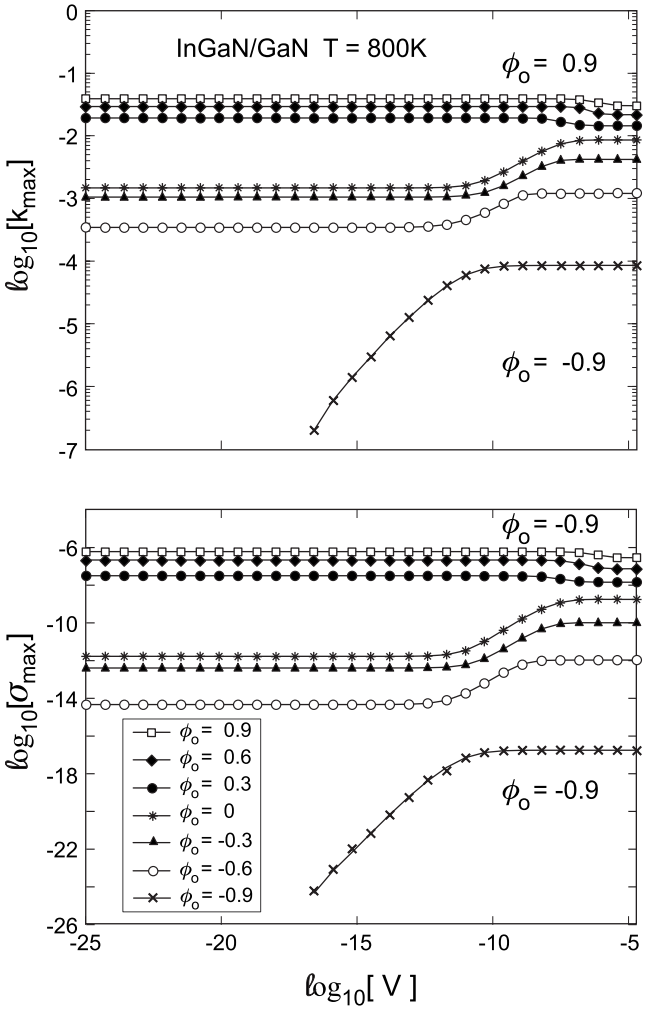

FIG. 10. InGaN/GaN films: k_{max} and σ_{max} vs V, at $T=800$ K, for various values of ϕ_o. From top to bottom, $\phi_o=0.9$ (squares), 0.6 (solid diamonds), 0.3 (solid circles), 0 (asterisks), −0.3 (solid triangles), −0.6 (open circles), and −0.9 (crosses).

$V\simeq 5\times10^{-10}$, 10^{-11}, 10^{-12}, 1.4×10^{-13}, and 3×10^{-14} for $T=500$, 600, 700, 800, and 900 K, respectively.

B. InGaP/GaAs

In contrast to Si-Ge/Si, GaAsN/GaAs, and InGaN/GaN, the InGaP film on a GaAs substrate is different in that neither InP nor GaP is its substrate. From Table I, it is seen that the lattice constant of GaAs is in between those of InP and GaP. For $\bar{\phi}^*=\phi_o^*=-0.0476$ corresponding to $In_{0.476}Ga_{0.524}P$ alloy film, there is an exact match between the lattice constants of the film and the substrate leading to $\epsilon(\phi_o^*)=0$. Around $\phi_o=\phi_o^*$, the morphological instability (arising from the lattice mismatch) is weak and the spinodal decomposition instability is either weaker or even is marginally stable for temperatures between 400 and 1000 K.

Figure 12 shows the variation in k_{max} and σ_{max} with V for an InGaP/GaAs film at 823 K for various values of ϕ_o. We choose $T=823$ K in order to make qualitative comparison to the experiments by Bortoleto *et al.*[30–32] A consistent general

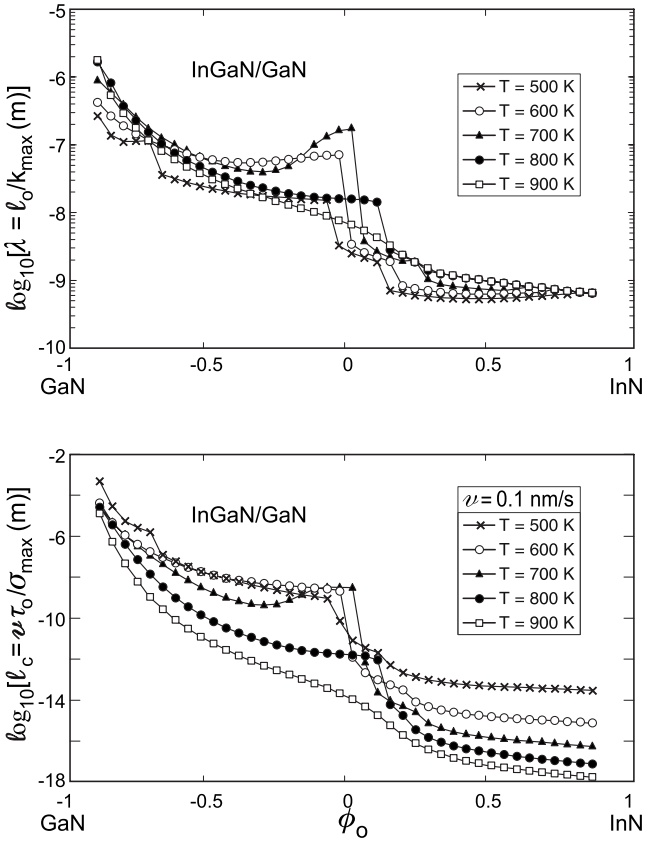

FIG. 11. InGaN/GaN films: λ and ℓ_c vs ϕ_o at various values of T as shown. The growth velocity is fixed at $v=0.1$ nm s^{-1}.

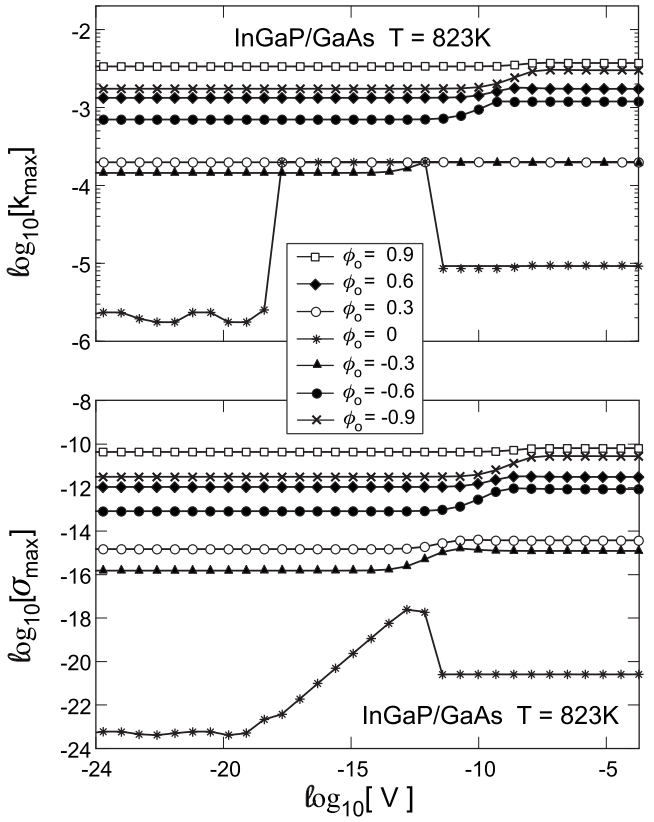

FIG. 12. InGaP/GaAs films: k_{max} and σ_{max} vs V, at $T=823$ K, for various values of ϕ_o. From top to bottom, $\phi_o=0.9$ (squares), 0.6 (solid diamonds), 0.3 (solid circles), 0 (asterisks), −0.3 (solid triangles), −0.6 (open circles), and −0.9 (crosses).

behavior common to Figs. 7, 10, and 12 is that the large V limit corresponding to the lattice mismatch root σ^{lm} is achieved by k_{max} and σ_{max} at the largest V shown in these figures. Figure 13 displays the variation in λ and ℓ_c with ϕ_o for various T at fixed growth velocity $v=0.1$ nm s^{-1}. For each T, as ϕ_o varies, the dimensionless V does not vary significantly: $V\simeq 4\times10^{-8}$, 5×10^{-10}, 2×10^{-11}, 2×10^{-12}, and 3×10^{-13} for $T=500$, 600, 700, 800, and 900 K, respectively. Around $\phi_o=\phi_o^*$, k_{max} and σ_{max} are almost zero leading to diverging λ and ℓ_c in Fig. 13. This behavior is also related to a narrow stability band for $\phi_o\geq\phi_o^*$ for various values of T as seen in Fig. 4.

Bortoleto *et al.*[30–32] have grown and examined InGaP/GaAs film samples (mostly at 823 K); three of these samples have $x=0.485$, 0.542, and 0.590 corresponding to $\phi_o=-0.03$, 0.084, and 0.18, respectively. For $\phi_o\simeq0.1$, from Fig. 13, $\lambda\simeq100$ nm which compares favorably to a value of 70 nm quoted by Bortoleto *et al.*[32] Even though the growth velocity v is higher, roughly by a factor of two, in these experiments, the values of λ and k_{max} are rather insensitive to variations in v for $v\geq0.1$ nm/s, as seen from Fig. 12.

V. CONCLUSIONS

In this paper, we investigated the nonequilibrium growth process of an epitaxially growing, coherent, asymmetric alloy film. We described in detail (Sec. II, Appendices A and B) a continuum dynamical model for asymmetric films which generalizes the work of Huang and Desai[25] for symmetric films. The model fully incorporates the long-range nature of the elastic forces by including the coupling of the top surface of a growing film with the bulk film underneath and the substrate below. The dependences of various parameters on the mean concentration x, appearing through the parameter ϕ_o ($\phi_o=2x-1$), is fully included. The role of concentration fluctuations around the mean is central to the model. The thermodynamic free energy for a binary mixture (mean-field model) is generalized to the appropriate Landau-Ginzburg (LG) free-energy functional, which leads to the alloy-segregation instability in mixtures with mean concentrations within the classical spinodal for $T<T_c$. The elastic free-energy functional is the cause of the morphological instability which arises from the film-substrate lattice mismatch. The two instabilities are coupled. In the model, the surface free-energy functional has a stabilizing effect on the growing film.

During the growth process, the film reaches mechanical and thermal equilibria on a much faster time scale than the chemical equilibrium. The assumption of instantaneous mechanical equilibrium is used to express the elastic displacement vector **u** in terms of the Fourier components of surface concentration fluctuations $\hat{\phi}_s$ and film height fluctuations $\hat{h}$; this expression is then used to eliminate **u** and to obtain a coupled set of linear equations of motion for $\hat{h}$ and $\hat{\phi}_s$. This set of equations quantifies the early stage of the film growth

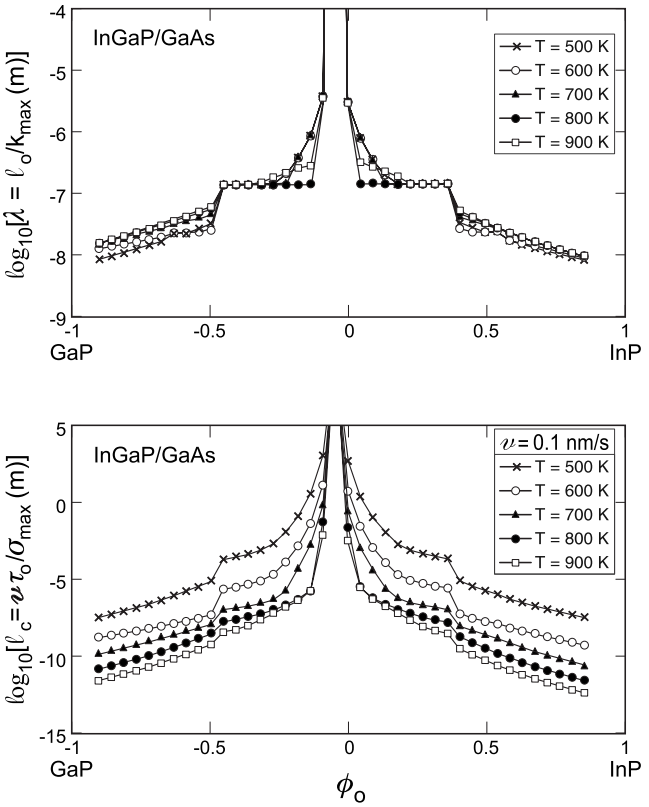

FIG. 13. InGaP/GaAs films: λ and ℓ_c vs ϕ_o at various values of T as shown. The growth velocity is fixed at v=0.1 nm s^{-1}.

as it evolves via the competition between deposition and surface diffusion. Characteristic length ℓ_o and characteristic time τ_o are defined and used to render the equations dimensionless in terms of $\hat{h}^*$ and $\hat{\phi}_s^*$.

The parameters in the model, none of which are adjustable, include the growth velocity V, lattice mismatch ϵ, solute-expansion coefficient η, mean order-parameter ϕ_o, and temperature T. Parameters related to material properties depend on ϕ_o and T; the dependence of ϵ and η on ϕ_o is shown in Fig. 1 for various films to which the theory is applied. The ϕ_o dependence of the elastic moduli E_o and μ_o; of the GL parameters r_e, u_e, and κ_e; of the characteristic lengths δ and ℓ_o; and of the characteristic time τ_o is also included in the numerical results shown in various figures. The parameters r_e and τ_o also depend on T. The sensitive T dependence of D_s and τ_o is shown in Fig. 2. There is significant uncertainty in the available experimental values of the effective surface-diffusion coefficient D_s; fortunately it enters the theory only through the characteristic time τ_o.

In Sec. III, the dimensionless linear coupled equations are used to perform a stability analysis. Various limiting cases, including the case of static films, are considered prior to the discussion of the general case. The case of ϵ=0 is illustrated in Fig. 3 with the InGaP/GaAs film which is lattice matched at ϕ_o=−0.0476. The stability phase diagram for four different static films is shown in Fig. 4. Figure 5 shows coupled instability related results for a static InGaN/GaN film. This is followed by the discussion of the analytic results for the general case. Figure 6 shows the importance of including the ϕ_o dependence of various parameters that enter the model. As a result of the coupling of the two instabilities, there is a joint modulation of the surface morphological profile and the alloy composition. Thus a planar surface can be stabilized only if alloy decomposition does not occur and vice versa.

The theory is applied to three semiconductor films—GaAsN/GaAs, InGaN/GaN, and InGaP/GaAs—in Sec. IV and the results are shown in Figs. 7–13. In Figs. 7, 10, and 12, the variations in dimensionless wave vector k_{max} and dimensionless growth exponent σ_{max} of the maximally unstable growth mode with respect to dimensionless growth velocity V are shown for a set of ϕ_o values. In Figs. 8, 11, and 13, the variations in the wavelength λ (in meters) of the maximally unstable mode and critical thickness ℓ_c (in meters) with respect to ϕ_o are shown for various temperatures T. Comparison with available experimental results is made. In applying the theory to asymmetric films, we find that the ϕ_o and T dependences of the model parameters make qualitative difference to the results. Due to uncertainty in values of D_s and τ_o, the absolute values of ℓ_c in Figs. 8, 11, and 13 may be in error, however, the trend of its variation with ϕ_o and T is expected to remain valid.

One of the shortcomings of the continuum theory, used in this paper, is that for the morphological instability it predicts a quadratic dependence on ϵ for the maximally unstable wave number k_{max}^{lm} [see Eq. (29) and the discussion following Eq. (30)], however, this result disagrees with experiments[48,49] on SiGe/Si(001) at temperatures around 950–1000 K, which shows a linear dependence of k_{max}^{lm} on ϵ. Some of the theoretical work[10,11,13,14] has explained these experimental results by considering differing atomic mobilities[82] of the constituent species on the film surface during the growth, especially as applied to the SiGe/Si film. This linear dependence may be more general as shown recently by Huang and Elder.[83] They used a multiple scale analysis to analyze a nonlinear phase field crystal model which incorporates continuum elasticity and crystalline symmetry and obtained the crossover from ϵ^2 to ϵ dependence for k_{max}^{lm}. It may be possible to extend our model by including these ideas.[10,83] However, the surface-diffusion process during the growth of asymmetric alloy films is complex, especially at temperatures $T<T_c$, for example, it can involve dimerized atoms and surface reconstruction.[84] The dimers, which may consist of either unlike or like alloy components, while diffusing on the growing film surface add to the complexity of the growth process.[85,86] Our model can also be extended along the lines of the work by Léonard and Desai,[21] if one needs to include atomic-ordering effects. Another simplification in our model is the assumption of elastic isotropy which simplified the elastic free-energy functional and analysis related to the mechanical equilibrium constraint. However most film materials are elastically anisotropic with zinc blende or wurtzite lattice structure. It may be possible to relax this assumption and extend the model to elastically anisotropic films with hexagonal or cubic lattice symmetry.[87]

ACKNOWLEDGMENTS

We acknowledge support by the NSERC of Canada and

the Department of Physics at University of Toronto, especially for the undergraduate summer research of H.K., D.N., S.C., and N.Y. R.C.D. would like to thank Zhi-Feng Huang for his helpful comments.

APPENDIX A: MECHANICAL EQUILIBRIUM CONSTRAINT

In this appendix, we use the condition of mechanical equilibrium to obtain[25] the displacement vector $\mathbf{u}$ and the strain tensor u_{ij} in terms of $\delta\phi$ and δh fields. We use the result to obtain, in Appendix B, the total free-energy functional to second order which, in turn, lets us obtain the linear dynamical equations for the 2D Fourier components of $\delta\phi$ and δh.

The displacement vector that enters the expression for the elastic free-energy density is measured from an appropriate reference state. Quantities that correspond to the reference state are indicated by an overbar. The system of interest, the coherent alloy film on top of a substrate, is heterogeneous for which the appropriate reference state has the substrate unconstrained and the coherent film constrained. This state corresponds to a uniform growing film with a homogeneous order-parameter $\bar{\phi}$ whose top surface is a planar front moving at a constant speed v corresponding to a thickness $\bar{h}=vt$. Coherency demands that the in-plane lattice constant of the film is the same as that of the substrate a_s and thus $\bar{u}^f_x=\bar{u}^f_y=0$. In the z direction, the Poisson relaxation leads to $\bar{u}^f_z=\bar{u}^f_{zz}z$ with $\bar{u}^f_{zz}\equiv\bar{u}=\epsilon(1+\nu^f)/(1-\nu^f)$. Here $\epsilon=(a_f-a_s)/a_s$ is the lattice mismatch, where a_f is the lattice constant of an unconstrained film. Note that both a_f and ϵ are functions of $\bar{\phi}$. The lattice mismatch leads to lateral stress in the film: $\bar{\sigma}^f_{xx}=\bar{\sigma}^f_{yy}\equiv\bar{\sigma}=-2\mu^f_o\bar{u}=-2\mu^f_o\epsilon(1+\nu^f)/(1-\nu^f)$. All the other components of strain and stress tensors in the film are zero for the reference state. The substrate is unconstrained and thus $\bar{u}^s_i=0$, $\bar{u}^s_{ij}=0$, and $\bar{\sigma}^s_{ij}=0$ for $i,j=x,y,z$ in the substrate for the reference state.

In absence of external forces, the condition of mechanical equilibrium is

$$\partial_j\sigma_{ij}=0, \tag{A1}$$

where the stress tensor, in the film, is

$$\sigma^f_{ij}=2\mu^f\left[\frac{\nu^f}{1-2\nu^f}u^f_{ll}\delta_{ij}+u^f_{ij}-\frac{1+\nu^f}{1-2\nu^f}(\epsilon+\eta\delta\phi)\delta_{ij}\right] \tag{A2}$$

and, in the substrate, it is

$$\sigma^s_{ij}=2\mu^s\left[\frac{\nu^s}{1-2\nu^s}u^s_{ll}\delta_{ij}+u^s_{ij}\right]. \tag{A3}$$

Here $\eta=(\partial a_f/\partial\phi)/a_f$ is the solute-expansion coefficient. Combining Eqs. (A1) and (A2), and using $u_{ij}=\frac{1}{2}(\partial_j u_i+\partial_i u_j)$, the mechanical equilibrium constraint on the displacement vector reduces to

$$\partial_i\partial_k u_k+(1-2\nu)\partial^2_k u_i-2(1+\nu)\eta\partial_i\delta\phi=0, \tag{A4}$$

in the film. In the substrate, the equation for u_i is the same as Eq. (A4) but without the term proportional to $\delta\phi$. The condition of mechanical equilibrium is supplemented by the following boundary conditions:

$$\sigma^f_{ij}n_j=0, \quad \text{at } z=h, \tag{A5}$$

indicating a free boundary with zero force at the top surface

$$\sigma^f_{zj}=\sigma^s_{zj}, \quad \text{at } z=0, \tag{A6}$$

indicating continuous stress at the film-substrate interface, and

$$\mathbf{u}^f=\mathbf{u}^s, \quad \text{at } z=0, \tag{A7}$$

corresponding to the continuity of displacement vector at $z=0$; and finally,

$$u^s_i\to 0 \quad \text{and} \quad u^s_{ij}\to 0 \text{ for } z\to-\infty, \tag{A8}$$

since the semi-infinite substrate is relaxed to equilibrium far away from the film-substrate interface. To solve for, it is convenient to use the 2D Fourier expansion of the variables

$$h=\bar{h}+\sum_{\mathbf{q}}\hat{h}(\mathbf{q},z,t)e^{i(q_x x+q_y y)}, \tag{A9a}$$

$$u^s_i=0+\sum_{\mathbf{q}}\hat{u}^s_i(\mathbf{q},z,t)e^{i(q_x x+q_y y)}, \tag{A9b}$$

$$u^f_i=\bar{u}^f_z\delta_{iz}+\sum_{\mathbf{q}}\hat{u}^f_i(\mathbf{q},z,t)e^{i(q_x x+q_y y)},$$

$$\text{where } \delta_{xz}=0, \quad \delta_{yz}=0, \quad \delta_{zz}=1, \tag{A9c}$$

$$\delta\phi=0+\sum_{\mathbf{q}}\hat{\phi}(\mathbf{q},z,t)e^{i(q_x x+q_y y)}. \tag{A9d}$$

Substituting Eqs. (A9a)–(A9d) in Eqs. (A4)–(A8), and using zeroth-order approximation of elastic constants, i.e., using $\nu^f_o=\nu^s_o=\nu_o$, we obtain

$$(1-2\nu_o)(\partial^2_z-q^2)\begin{bmatrix}\hat{u}^f_x\\ \hat{u}^f_y\\ \hat{u}^f_z\end{bmatrix}+\begin{bmatrix}iq_x\\ iq_y\\ \partial_z\end{bmatrix}\times[iq_x\hat{u}^f_x+iq_y\hat{u}^f_y+\partial_z\hat{u}^f_z-2(1+\nu_o)\eta\hat{\phi}]=0, \tag{A10}$$

where $q^2=q^2_x+q^2_y$. The equation for the substrate displacement $\mathbf{u}^s$ is similar to Eq. (A10), but the inhomogeneous term $2(1+\nu_o)\eta\hat{\phi}$ is absent. The boundary condition at $z=h$ reduces to

$$\hat{\sigma}^f_{xz}=iq_x\bar{\sigma}\hat{h}; \quad \hat{\sigma}^f_{yz}=iq_y\bar{\sigma}\hat{h}; \quad \text{and} \quad \hat{\sigma}^f_{zz}=0. \tag{A11}$$

The boundary conditions at $z=0$ reduce to

$$\hat{\sigma}^f_{iz}=\hat{\sigma}^s_{iz} \text{ for } i=x,y,z, \tag{A12}$$

$$\hat{u}^f_i=\hat{u}^s_i \text{ for } i=x,y,z. \tag{A13}$$

Finally, the boundary conditions at $z=-\infty$ reduce to

$$\hat{u}_i^s \to 0 \quad \text{and} \quad \partial_z \hat{u}_i^s \to 0. \tag{A14}$$

The solution of Eqs. (A10)–(A14) has been obtained by Huang and Desai.[25] In the film, it is

$$\hat{u}_i^f = \begin{bmatrix} \alpha_x \\ \alpha_y \\ \alpha_z \end{bmatrix} e^{qz} - \begin{bmatrix} iq_x/q \\ iq_y/q \\ 1 \end{bmatrix} Cze^{qz} + \left(\frac{1+\nu_o}{1-\nu_o}\right)\eta \begin{bmatrix} iq_x\hat{W} \\ iq_y\hat{W} \\ \partial_z\hat{W} \end{bmatrix}. \tag{A15}$$

The coefficients α_i and C are given by

$$q_y\alpha_x = q_x\alpha_y, \tag{A16}$$

$$iq_x\alpha_x + iq_y\alpha_y = e^{-q\bar{h}}\left\{[2(1-\nu_o) - q\bar{h}]\left[q\bar{u}\hat{h} + \left(\frac{1+\nu_o}{1-\nu_o}\right)\eta q(\partial_z\hat{W})_{z=\bar{h}}\right] + (-1+2\nu_o+q\bar{h}) \times \left(\frac{1+\nu_o}{1-\nu_o}\right)\eta(\partial_z^2\hat{W} - \hat{\phi})_{z=\bar{h}}\right\}, \tag{A17}$$

$$q\alpha_z = e^{-q\bar{h}}\left\{(1-2\nu_o+q\bar{h})\left[q\bar{u}\hat{h} + \left(\frac{1+\nu_o}{1-\nu_o}\right)\eta q(\partial_z\hat{W})_{z=\bar{h}}\right] - [2(1-\nu_o)+q\bar{h}]\left(\frac{1+\nu_o}{1-\nu_o}\right)\eta(\partial_z^2\hat{W} - \hat{\phi})_{z=\bar{h}}\right\}, \tag{A18}$$

$$C = e^{-q\bar{h}}\left[q\bar{u}\hat{h} + \left(\frac{1+\nu_o}{1-\nu_o}\right)\eta(q\partial_z\hat{W} - \partial_z^2\hat{W} + \hat{\phi})_{z=\bar{h}}\right]. \tag{A19}$$

Here one can understand how the Green's function $\hat{W}$ is introduced through the particular solution of the mechanical equilibrium equation by taking a divergence of Eq. (A4). If one then introduces the relation $\nabla^2 W = \delta\phi$ in real space,[22] and uses $W(x,y,z,t) = \Sigma_{\mathbf{q}}\hat{W}(\mathbf{q},z,t)e^{i(q_x x + q_y y)}$, one has

$$(\partial_z^2 - q^2)\hat{W}(\mathbf{q},z,t) = \hat{\phi} \tag{A20}$$

in Fourier space. This, in turn, leads to the particular solution of Eq. (A10) given by the last term of Eq. (A15). Corresponding to the frozen, buried, metastable layers of the film, one can substitute $\hat{\phi} = \hat{\phi}_o(\mathbf{q})e^{\Omega t}$, with $t = z/v$, to obtain the expression of $\hat{W}$

$$\hat{W} = \frac{v^2\hat{\phi}_o}{\Omega^2 - (qv)^2}e^{\Omega z/v}. \tag{A21}$$

Equations (A15)–(A21) give the displacement vector $\mathbf{u}$ in terms of $\hat{h}$ and $\hat{\phi}$.

APPENDIX B: FREE-ENERGY FUNCTIONAL TO SECOND-ORDER AND LINEAR DYNAMICAL EQUATIONS

The elastic free-energy functional can be written, using Eqs. (11) and (A2), as

$$\mathcal{F}_{\text{el}}^f = \int dx \int dy \int_0^h dz \left[\frac{1}{2}\lambda^f u_{ll}^{f\,2} + \mu^f u_{ij}^{f\,2} + \frac{E^f}{1-2\nu^f}\left(\frac{3}{2}\epsilon^2 - \epsilon u_{ll}^f + 3\epsilon\eta\delta\phi + \frac{3}{2}\eta^2\delta\phi^2 - \eta\delta\phi u_{ll}^f\right)\right] \tag{B1}$$

with the Lamé coefficient $\lambda^f = 2\mu^f\nu^f/(1-2\nu^f)$. Since from Eq. (13) both Young's and Shear moduli depend on composition fluctuations, we can write Eq. (B1) to first order in E_1^* and μ_1^* as

$$\mathcal{F}_{\text{el}}^f = \int dx \int dy \int_0^h dz \left\{\frac{1}{2}\lambda_o u_{ll}^{f\,2} + \mu_o u_{ij}^{f\,2} + \mu_o\mu_1^*\delta\phi u_{ij}^{f\,2} + \frac{E_o}{1-2\nu_o}\left[\frac{3}{2}\epsilon^2 - \epsilon u_{ll}^f + 3\left(\epsilon\eta + \frac{3E_1^* - 2(1+\nu_o)\mu_1^*}{2(1-2\nu_o)}\epsilon^2\right)\delta\phi + 3\left(\frac{1}{2}\eta^2 + \frac{3E_1^* - 2(1+\nu_o)\mu_1^*}{1-2\nu_o}\epsilon\eta\right)\delta\phi^2 - \left(\eta + \frac{3E_1^* - 2(1+\nu_o)\mu_1^*}{1-2\nu_o}\epsilon\right)\delta\phi u_{ll}^f + \frac{1}{2(1-2\nu_o)}\left(E_1^* - \frac{1+2\nu_o^2}{1+\nu_o}\mu_1^*\right)\delta\phi u_{ll}^{f\,2} - \frac{3E_1^* - 2(1+\nu_o)\mu_1^*}{1-2\nu_o}\eta\delta\phi^2 u_{ll}^f + \frac{3}{2}\left(\frac{3E_1^* - 2(1+\nu_o)\mu_1^*}{1-2\nu_o}\right)\eta^2\delta\phi^3\right]\right\} \tag{B2}$$

with $\lambda_o = 2\mu_o\nu_o/(1-2\nu_o)$. The Fourier expansion to second order of the elastic free-energy functional given in Eq. (B2) can be obtained.[25] It is

$$\mathcal{F}_{\rm el}^f = \int dx \int dy \int_0^h dz \left[\bar{\mathcal{E}}^f + \sum_{\mathbf{q}} e^{i(q_x x + q_y y)} \hat{\mathcal{E}}^f(q,z,t) \right] + \tilde{\mathcal{F}}_{\rm el}^f. \tag{B3}$$

Here the zeroth-order term

$$\bar{\mathcal{E}}^f = \frac{E_o}{1-\nu_o} \epsilon^2 \tag{B4}$$

does not contribute to the dynamic Eqs. (5) and (6). The first-order term is

$$\hat{\mathcal{E}}^f = \frac{E_o}{1-\nu_o} \epsilon \left[-\hat{u}_{ll}^f + \hat{u}_{zz}^f + \left(2\eta + \frac{2E_1^* - (1+\nu_o)\mu_1^*}{1-\nu_o} \epsilon \right) \hat{\phi} \right] \tag{B5}$$

and the second-order term is

$$\begin{aligned} \tilde{\mathcal{F}}_{\rm el}^f = \sum_{\mathbf{q}} \int_0^{\bar{h}} dz \Bigg\{ \frac{E_o}{1-2\nu_o} \Bigg[& \left(\frac{3}{2}\eta^2 + \frac{2(3E_1^* - 2(1+\nu_o)\mu_1^*)}{1-\nu_o} \epsilon\eta \right) \hat{\phi}(\mathbf{q}) \hat{\phi}(-\mathbf{q}) \\ & - \left(\eta + \frac{2E_1^* - (1+2\nu_o)\mu_1^*}{1-\nu_o} \epsilon \right) \hat{\phi}(\mathbf{q}) \hat{u}_{ll}^f(-\mathbf{q}) \\ & + \frac{\nu_o}{2(1+\nu_o)} \hat{u}_{ll}^f(\mathbf{q}) \hat{u}_{ll}^f(-\mathbf{q}) \Bigg] + \frac{E_o}{1-\nu_o} \mu_1^* \epsilon \hat{\phi}(\mathbf{q}) \hat{u}_{zz}^f(-\mathbf{q}) \\ & + \frac{E_o}{2(1+\nu_o)} \hat{u}_{ij}^f(\mathbf{q}) \hat{u}_{ij}^f(-\mathbf{q}) \Bigg\}. \end{aligned} \tag{B6}$$

These terms contain various strain tensor component combinations: $\hat{u}_{ij}^f$, $\hat{u}_{ll}^f$, and $\hat{u}_{zz}^f$. These can be determined from the solution for the displacement vector $\mathbf{u}$ obtained in Appendix A. The strain tensor u_{ij}^f is composed of two parts: $u_{ij}^f = u_{ij}^{hom} + u_{ij}^{par}$, the homogeneous solution and the particular solution. Since the homogeneous part is not the function of either of the system variables ϕ or W, and the coefficients α_i and C only depend on the surface values evaluated at $z=\bar{h}$, it does not contribute to the functional derivative of the elastic free energy with respect to ϕ. For the functional derivative only the particular solution of strain tensor needs to be considered[25]

$$u_{ij}^{par} = \frac{1+\nu_o}{1-\nu_o} \eta \partial_i \partial_j W. \tag{B7}$$

The Fourier space quantities $\hat{u}_{ll}^f$ and $\hat{u}_{zz}^f$ can also be calculated from $\hat{u}_i^f$ given in Appendix A and are

$$\hat{u}_{ll}^f = 2(1-2\nu_o^f) C e^{qz} + \left(\frac{1+\nu_o^f}{1-\nu_o^f} \right) \eta \hat{\phi},$$

$$\hat{u}_{zz}^f = q\alpha_z e^{qz} - C(1+qz)e^{qz} + \left(\frac{1+\nu_o^f}{1-\nu_o^f} \right) \eta \partial_z^2 \hat{W}, \tag{B8}$$

where α_z, C, and $\hat{W}$ are as in Eqs. (A18)–(A21). Together Eqs. (B4)–(B6) provide the elastic free-energy functional to second order. Along with the surface free-energy $\mathcal{F}_s$ in Eq. (9) and the Landau-Ginzburg free energy $\mathcal{F}_{\rm LG}$ in Eq. (12), one has the total free-energy functional explicitly to second order. These can be substituted in the coupled dynamical Eqs. (5) and (6) to obtain the linearized equations for $\hat{\phi}$ and $\hat{h}$. In terms of Fourier transformed variables, Eq. (5) is

$$\frac{\partial \hat{h}}{\partial t} = -\Gamma_h q^2 \left\{ \gamma q^2 \hat{h} + \left[\frac{\delta \mathcal{F}_{\rm el}}{\delta(\delta h)} \right]_q + \left[\frac{\delta \mathcal{F}_{\rm LG}}{\delta(\delta h)} \right]_q \right\}. \tag{B9}$$

Using Eq. (B3),

$$\frac{\delta \mathcal{F}_{\rm el}}{\delta(\delta h)} = \frac{\delta}{\delta(\delta h)} \int dx \int dy \int_0^h dz \left[\bar{\mathcal{E}}^f + \sum_{\mathbf{q}} e^{i(q_x x + q_y y)} \hat{\mathcal{E}}^f(q,z,t) \right] + \text{higher order terms}. \tag{B10}$$

Keeping terms up to the first order, this is equal to $[\bar{\mathcal{E}}^f + \Sigma_{\mathbf{q}} e^{i(q_x x + q_y y)} \hat{\mathcal{E}}^f(q,z,t)]_{z=h}$, where the subscript $z=h$ indicates that quantities are calculated at the top film surface. Due to the overall Laplacian in Eq. (5) or equivalently due to q^2 in Eq. (B9), the constant term $\bar{\mathcal{E}}^f$ does not contribute. Thus to first order

$$\left(\frac{\delta \mathcal{F}_{\rm el}}{\delta(\delta h)} \right)_q \Rightarrow \hat{\mathcal{E}}^f|_s = \frac{E_o}{1-\nu_o} \epsilon \left[-2(1+\nu_o)\epsilon q \hat{h} + \left(2\eta \frac{\Omega - \nu_o q v}{\Omega + q v} + \frac{\alpha_o}{1-\nu_o} \epsilon \right) \hat{\phi}_s \right], \tag{B11}$$

where $\hat{\phi}|_{z=h} = \hat{\phi}_s$ to first order and $\alpha_o = 2E_1^* - (1+\nu_o)\mu_1^*$. From Eq. (12), we obtain the last term in Eq. (B9), to first order, as

$$\left(\frac{\delta \mathcal{F}_{\rm LG}}{\delta(\delta h)} \right)_q = \frac{\delta}{\delta(\delta h)} \int dx \int dy \int_0^h dz [f_{\rm LG}] = [f_{\rm LG}]_{z=h} = (-r'\phi_o + u\phi_o^3)\hat{\phi}_s. \tag{B12}$$

Thus the linearized dynamical equation for $\hat{h}(q,t)$ is

$$\begin{aligned} \frac{\partial \hat{h}}{\partial t} = & -\Gamma_h q^2 \{ \gamma q^2 - 2E_o \chi q \epsilon^2 \} \hat{h} \\ & - \Gamma_h q^2 \left\{ \frac{E_o}{1-\nu_o} \left(\frac{\alpha_o \epsilon^2}{1-\nu_o} + 2\epsilon\eta \frac{\Omega - \nu_o q v}{\Omega + q v} \right) - r'\phi_o + u\phi_o^3 \right\} \hat{\phi}_s, \end{aligned} \tag{B13}$$

where $\chi = (1+\nu_o)/(1-\nu_o)$. Note that in Eq. (B6), $\tilde{\mathcal{F}}_{\rm el}^f$ is independent of $\hat{h}$; thus the second-order term does not contribute to $\frac{\partial \hat{h}}{\partial t}$, since $(\frac{\delta \tilde{\mathcal{F}}_{\rm el}^f}{\delta(\delta h)})_q$ vanishes. For the linearized dynamical equation for $\hat{\phi}(q, z=h, t) \equiv \hat{\phi}_s(q,t)$, both the first and the second-order terms in Eqs. (B5) and (B6) contribute, as well as the $\mathcal{F}_{\rm LG}$ from Eq. (12). The result is

$$\frac{\partial \hat{\phi}_s}{\partial t} = -\Gamma_\phi q^2(-r' + 3u\phi_o^2 + \kappa q^2)\hat{\phi}_s - \Gamma_\phi q^2 \frac{2E_o}{1-\nu_o}\left(\eta^2 + \beta_o \epsilon\eta - \frac{qv}{\Omega + qv}\chi\{(1-2\nu_o)\eta^2 + \alpha_o \epsilon\eta\}\right)\hat{\phi}_s$$

$$-\Lambda\hat{\phi}_s + \Gamma_\phi q^3 \frac{2E_o}{1-\nu_o}\chi\{(1-2\nu_o)\eta\epsilon + \alpha_o\epsilon^2\}\hat{h}_s, \tag{B14}$$

where $\beta_o = [8E_1^* - 5(1+\nu_o)\mu_1^*]/[2(1-\nu_o)]$. If we set $\phi_o = 0$ in Eqs. (B13) and (B14), we recover the results for the case of a symmetric alloy considered by Huang and Desai.[25]

*desai@physics.utoronto.ca
†swmelon@gmail.com
‡Permanent address: IISER-Pune, Pashan, Pune 411021, Maharashtra, India; apratim@iiserpune.ac.in
§darryl.ngai@utoronto.ca
‖siannie.chen@utoronto.ca
¶n.yang@utoronto.ca

[1] R. J. Asaro and W. A. Tiller, Metall. Trans. **3**, 1789 (1972).
[2] M. A. Grinfeld, Sov. Phys. Dokl. **31**, 831 (1987).
[3] D. J. Srolovitz, Acta Metall. **37**, 621 (1989).
[4] B. J. Spencer, P. W. Voorhees, and S. H. Davis, J. Appl. Phys. **73**, 4955 (1993); Phys. Rev. Lett. **67**, 3696 (1991).
[5] H. Gao, J. Mech. Phys. Solids **42**, 741 (1994); Annu. Rev. Mater. Sci. **29**, 173 (1999).
[6] V. A. Shchukin and D. Bimberg, Rev. Mod. Phys. **71**, 1125 (1999); B. Teichert, Phys. Rep. **365**, 335 (2002); A. Stangl, V. Holy, and G. Bauer, Rev. Mod. Phys. **76**, 725 (2004).
[7] R. C. Desai and R. Kapral, *Dynamics of Self-Organized and Self-Assembled Structures* (Cambridge University Press, Cambridge, 2009), Chap. 17
[8] J. W. Cahn, Acta Metall. **9**, 795 (1961); Trans. Metall. Soc. AIME **242**, 166 (1968); Acta Metall. **7**, 18 (1959).
[9] Y. Tu and J. Tersoff, Phys. Rev. Lett. **93**, 216101 (2004); **98**, 096103 (2007).
[10] B. J. Spencer, P. W. Voorhees, and J. Tersoff, Phys. Rev. B **64**, 235318 (2001).
[11] B. J. Spencer, P. W. Voorhees, and J. Tersoff, Appl. Phys. Lett. **76**, 3022 (2000).
[12] B. J. Spencer, P. W. Voorhees, and J. Tersoff, Phys. Rev. Lett. **84**, 2449 (2000).
[13] J. Tersoff, Phys. Rev. Lett. **85**, 2843 (2000).
[14] P. Venezuela and J. Tersoff, Phys. Rev. B **58**, 10871 (1998).
[15] J. Tersoff, Phys. Rev. B **56**, R4394 (1997).
[16] J. E. Guyer and P. W. Voorhees, Phys. Rev. B **54**, 11710 (1996).
[17] J. E. Guyer and P. W. Voorhees, in *Evolution of Epitaxial Structure and Morphology*, MRS Symposia Proceedings No. 399, edited by A. Zangwill, and D. Jesson, D. Chambliss, and R. Clarke (Materials Research Society, Pittsburgh, 1996), p. 351.
[18] J. E. Guyer and P. W. Voorhees, Phys. Rev. Lett. **74**, 4031 (1995).
[19] J. Tersoff and F. K. LeGoues, Phys. Rev. Lett. **72**, 3570 (1994).
[20] F. Léonard and R. C. Desai, Appl. Phys. Lett. **74**, 40 (1999).
[21] F. Léonard and R. C. Desai, Appl. Phys. Lett. **73**, 208 (1998).
[22] F. Léonard and R. C. Desai, Phys. Rev. B **57**, 4805 (1998).
[23] F. Léonard and R. C. Desai, Phys. Rev. B **56**, 4955 (1997).
[24] F. Léonard and R. C. Desai, Phys. Rev. B **55**, 9990 (1997).
[25] Z. F. Huang and R. C. Desai, Phys. Rev. B **65**, 205419 (2002).
[26] Z. F. Huang and R. C. Desai, Phys. Rev. B **65**, 195421 (2002).
[27] P. Henoc, A. Izrael, M. Quillec, and H. Launois, Appl. Phys. Lett. **40**, 963 (1982).
[28] O. Ueda, S. Isozumi, and S. Komiya, Jpn. J. Appl. Phys., Part 2 **23**, L241 (1984).
[29] R. R. LaPierre, T. Okada, B. J. Robinson, D. A. Thompson, and G. C. Weatherly, J. Cryst. Growth **158**, 6 (1996).
[30] J. R. R. Bortoleto, H. R. Gutierrez, M. A. Cotta, and J. Bettini, J. Appl. Phys. **101**, 064907 (2007).
[31] J. R. R. Bortoleto, H. R. Gutierrez, M. A. Cotta, and J. Bettini, Appl. Phys. Lett. **87**, 013105 (2005).
[32] J. R. R. Bortoleto, H. R. Gutierrez, M. A. Cotta, J. Bettini, L. P. Cardoso, and M. M. G. de Carvalho, Appl. Phys. Lett. **82**, 3523 (2003).
[33] C. D. Adams, M. Atzmon, Y.-T. Cheng, and D. J. Srolovitz, J. Mater. Res. **7**, 653 (1992).
[34] G. C. Hua, N. Otsuka, D. C. Grillo, J. Han, L. He, and R. L. Gunshor, J. Cryst. Growth **138**, 367 (1994).
[35] S. R. Lee, D. D. Koleske, K. C. Cross, J. A. Floro, K. E. Waldrip, A. T. Wise, and S. Mahajan, Appl. Phys. Lett. **85**, 6164 (2004); F. Y. Meng, M. Rao, N. Newman, and S. Mahajan, Acta Mater. **56**, 5552 (2008).
[36] S. M. de Sousa Pereira, K. P. O'Donnell, and E. Alves, Adv. Funct. Mater. **17**, 37 (2007).
[37] Z. Liliental-Weber, D. N. Zakharov, K. M. Yu, J. W. Ager III, W. Walukiewicz, E. H. Haller, H. Lu, and W. J. Schaff, J. Electron Microsc. **54**, 243 (2005).
[38] M. Rao, D. Kim, and S. Mahajan, Appl. Phys. Lett. **85**, 1961 (2004); A. N. Westmeyer and S. Mahajan, *ibid.* **79**, 2710 (2001).
[39] D. Doppalapudi, S. N. Basu, K. F. Ludwig, Jr., and T. D. Moustakas, J. Appl. Phys. **84**, 1389 (1998).
[40] J. E. Guyer, S. A. Barnett, and P. W. Voorhees, J. Cryst. Growth **217**, 1 (2000).
[41] N. S. Chokshi and J. M. Millunchick, Appl. Phys. Lett. **76**, 2382 (2000).
[42] J. Mirecki Millunchick, R. D. Twesten, D. M. Follstaedt, S. R. Lee, E. D. Jones, Y. Zhang, S. P. Ahrenkiel, and A. Mascarenhas, Appl. Phys. Lett. **70**, 1402 (1997); S. P. Ahrenkiel, A. G. Norman, M. M. Al-Jassim, A. Mascarenhas, J. Mirecki Millunchick, R. D. Twesten, S. R. Lee, D. M. Follstaedt, and E. D. Jones, J. Appl. Phys. **84**, 6088 (1998).
[43] J.-M. Baribeau and X. Wu, Phys. Can. **63**, 23 (2007).
[44] A. Marzegalli, V. A. Zinovyev, F. Montalenti, A. Rastelli, M. Stoffel, T. Merdzhanova, O. G. Schmidt, and L. Miglio, Phys. Rev. Lett. **99**, 235505 (2007).
[45] L. Huang, F. Liu, G.-H. Lu, and X. G. Gong, Phys. Rev. Lett. **96**, 016103 (2006).

[46] E. Sutter, P. Sutter, and J. E. Bernard, Appl. Phys. Lett. **84**, 2262 (2004).
[47] C. Schelling, G. Springholz, and F. Schaffler, Thin Solid Films **380**, 20 (2000).
[48] P. Sutter and M. G. Lagally, Phys. Rev. Lett. **84**, 4637 (2000); see also Ref. 13.
[49] R. M. Tromp, F. M. Ross, and M. C. Reuter, Phys. Rev. Lett. **84**, 4641 (2000).
[50] H. Lafontaine, B. F. Mason, S. J. Rolfe, D. D. Perović, and B. Bahierathan, J. Vac. Sci. Technol. B **16**, 599 (1998).
[51] D. D. Perović, B. Bahierathan, H. Lafontaine, D. C. Houghton, and D. W. McComb, Physica A **239**, 11 (1997).
[52] T. Walther, C. J. Humphreys, and A. G. Cullis, Appl. Phys. Lett. **71**, 809 (1997).
[53] J. Tersoff, C. Teichert, and M. G. Lagally, Phys. Rev. Lett. **76**, 1675 (1996).
[54] Y. H. Xie, G. H. Gilmer, C. Roland, P. J. Silverman, S. K. Buratto, J. Y. Cheng, E. A. Fitzgerald, A. R. Kortan, S. Schuppler, M. A. Marcus, and P. H. Citrin, Phys. Rev. Lett. **73**, 3006 (1994).
[55] D. E. Jesson, S. J. Pennycook, J. Z. Tischler, J. D. Budai, J.-M. Baribeau, and D. C. Houghton, Phys. Rev. Lett. **70**, 2293 (1993); D. E. Jesson, S. J. Pennycook, J.-M. Baribeau, and D. C. Houghton, Phys. Rev. Lett. **71**, 1744 (1993); **71**, 3737 (1993).
[56] See, for example, S. Nakamura, MRS Bull. **23**, 37 (1998).
[57] Electronic archive New Semiconductor Materials. Characteristics and Properties, Ioffe Physico-Technical Institute, http://www.ioffe.rssi.ru/SVA/NSM/
[58] O. Brandt, H. Yang, and K. H. Ploog, Phys. Rev. B **54**, 4432 (1996).
[59] Using solid source MBE, M. A. Pinault and E. Tournie, Appl. Phys. Lett. **79**, 3404 (2001) grew GaAsN/GaAs films with 2.8% nitrogen content between 663 and 753 K, and examined the consequences of alloy stability.
[60] S. B. Zhang and S.-H. Wei, Phys. Rev. Lett. **86**, 1789 (2001).
[61] Y. Qiu, S. A. Nikishin, H. Temkin, V. A. Elyukhin, and Yu. A. Kudriatsev, Appl. Phys. Lett. **70**, 2831 (1997).
[62] H. Kim and T. G. Andersson, Appl. Phys. Lett. **80**, 4768 (2002).
[63] W. M. McGee, R. S. Williams, M. J. Ashwin, T. S. Jones, E. Clarke, J. Zhang, and S. Tomić, Phys. Rev. B **76**, 085309 (2007).
[64] W. W. Mullins, J. Appl. Phys. **28**, 333 (1957).
[65] M. Atzmon, D. A. Kessler, and D. J. Srolovitz, J. Appl. Phys. **72**, 442 (1992).
[66] Z.-F. Huang and R. C. Desai, Phys. Rev. B **67**, 075416 (2003).
[67] Z.-F. Huang, D. Kandel, and R. C. Desai, Appl. Phys. Lett. **82**, 4705 (2003).
[68] O. Caha, V. Holy, and K. E. Bassler, Phys. Rev. Lett. **96**, 136102 (2006); O. Caha, P. Mikulik, J. Novak, V. Holy, S. C. Moss, A. Norman, A. Mascarenhas, J. L. Reno, and B. Krause, Phys. Rev. B **72**, 035313 (2005).
[69] Three of the four alloy systems considered have one of the components as the substrate: the growth of Si-Ge/Si at $\phi=1$, GaAsN/GaAs at $\phi=-1$ and InGaN/GaN at $\phi=-1$ would correspond to the limit of homoepitaxy. Ehrlich-Schwoebel barriers near step edges play important role in such systems, e.g., epitaxially growing Si film on a Si substrate; in our analysis, we have not included the nonequilibrium surface diffusion current that is associated with these barriers. See J. Krug, M. Plischke, and M. Siegert, Phys. Rev. Lett. **70**, 3271 (1993); J. Krug, Adv. Phys. **46**, 139 (1997).
[70] The natural structure for GaN is wurtzite. However, high quality, bulk, free-standing, zinc blende cubic GaN crystals have been grown by plasma-assisted MBE. See S. V. Novikov, N. M. Stanton, R. P. Campion, R. D. Morris, H. S. Green, C. T. Foxton, and A. J. Kent, Semicond. Sci. Technol. **23**, 015018 (2008); Such free- standing GaN crystals make ideal, nearly lattice matched substrates for the growth of InGaN films which are useful for UV optoelectronic devices and for high-power and high-frequency electronic applications. Also undoped thick cubic GaN fims have been grown on semi-insulating GaAs(001) substrates using plasma-assisted MBE by L. C. Jenkins, T. S. Cheng, C. T. Foxon, J. W. Orton, S. E. Hooper, S. V. Novikov, and V. V. Tret'yakov, J. Vac. Sci. Technol. B **13**, 1585 (1995).
[71] A. F. Wright, J. Appl. Phys. **82**, 2833 (1997).
[72] U. Rössler and D. Strauch, *Semiconductors, Group IV Elements, IV-IV and III-V Compounds, Lattice Properties*, edited by W. Martienssen, Landolt-Börnstein, New Series, Group III, Vol. 41, Part α (Springer, Berlin, 2001).
[73] J. E. Ayers, *Heteroepitaxy of Semiconductors* (CRC Press, Boca Raton, 2007), pp. 35–36.
[74] L. Vegard, Z. Phys. **5**, 17 (1921; Significant departures from the linear interpolation of Vegard's law has been seen theoretically and experimentally; see for example, M. Reason, X. Weng, W. Ye, D. Dettling, S. Hanson, G. Obeidi, and R. S. Goldman, J. Appl. Phys. **97**, 103523 (2005).
[75] F. C. Larché and J. W. Cahn, Acta Metall. **33**, 331 (1985).
[76] C. K. Gan, Y. P. Feng, and D. J. Srolovitz, Phys. Rev. B **73**, 235214 (2006); see Fig. 5(b).
[77] S. Y. Karpov, N. I. Podolskaya, I. A. Zhmakin, and A. I. Zhmakin, Phys. Rev. B **70**, 235203 (2004).
[78] K. Ishida, T. Nomura, H. Tokunaga, H. Ohtani, and T. Nishizawa, J. Less-Common Met. **155**, 193 (1989); H. Ho and G. B. Stringfellow, Appl. Phys. Lett. **69**, 2701 (1996).
[79] I. V. Rogozin and A. N. Georgobiani, Inorg. Mater. **42**, 1342 (2006).
[80] In the GaAsN film, when viewed as a mixture of GaAs and GaN, it is the relative diffusion of As and N that is relevant which makes the motion of lighter N atoms important. On the other hand, in the InGaN≡(InN+GaN) and InGaP≡(InP+GaP) films, due to the relative diffusion of In and Ga, the motion of Ga becomes important; for this, see Ref. 58 and M. H. Yang and C. P. Flynn, Phys. Rev. Lett. **62**, 2476 (1989); see also, S. A. Kukushkin, V. N. Bessolov, A. V. Osipov, and A. V. Luk'yanov, Phys. Solid State **43**, 2229 (2001); **44**, 1399 (2002); and T. Okumura and Y. Akagi, J. Appl. Phys. **90**, 5515 (2001) for a novel approach for inferring D_s from experiments on the early stages of phase separation.
[81] Note that due to uncertainties in D_s, values deduced for τ_o are uncertain. In turn, these introduce uncertainties in the critical thickness ℓ_c. In spite of this, we expect the overall trends to be as shown in Figs. 8, 11, and 13.
[82] S. J. Chey and D. G. Cahill, *Dynamics of Crystal Surfaces and Interfaces*, edited by Duxbury and Pence (Plenum Press, New York, 1997), p. 59.
[83] Z.-F. Huang and K. R. Elder, Phys. Rev. Lett. **101**, 158701 (2008).
[84] The surface reconstruction effects considered here mainly apply to the ultra-high vacuum growth like MBE, while for the growing processes under hydrogen environment, such as CVD, the

dimer formation is prevented due to the passivation effect of hydrogen on the dangling bonds, and then the corresponding diffusion kinetics are different from that discussed in this paper. See, e.g., C. S. Ozkam, W. D. Nix, and H. Gao, in *Structure and Evolution of Surfaces*, MRS Symposia Proceedings No. 440, edited by R. C. Cammarata, E. H. Chason, T. L. Einstein, and E. D. Williams (Materials Research Society, Pittsburgh, 1997), p. 323.

[85] H. J. W. Zandvliet, B. Poelsema, and B. S. Swartzentruber, Phys. Today **54** (7), 40 (2001).

[86] X. R. Qin, B. S. Swartzentruber, and M. G. Lagally, Phys. Rev. Lett. **85**, 3660 (2000).

[87] R. C. Desai and S. Chen (unpublished).